

An X-ray spectral survey of the disc of M31 with XMM-Newton

L. Shaw Greening¹, R. Barnard¹, U. Kolb¹, C. Tonkin¹, and J.P. Osborne²

¹ The Department of Physics and Astronomy, The Open University, Walton Hall, Milton Keynes, MK7 6AA, UK

² The Department of Physics and Astronomy, The University of Leicester, Leicester, LE1 7RH, UK

Received date / Accepted date

ABSTRACT

Aims. We present the results of a complete spectral survey of the X-ray point sources detected in five XMM-Newton observations along the major axis of M31 but avoiding the central bulge, aimed at establishing the population characteristics of X-ray sources in this galaxy.

Methods. We obtained background subtracted spectra and lightcurves for each of the 335 X-ray point sources detected across the five observations from 2002. We also correlate our source list with those of earlier X-ray surveys and radio, optical and infra-red catalogues. Sources with more than 50 source counts are individually spectrally fit in order to create the most accurate luminosity functions of M31 to date.

Results. Based on the spectral fitting of these sources with a power law model, we observe a broad range of best fit photon index. From this distribution of best fit index, we identify 16 strong high mass X-ray binary system candidates in M31. We show the first cumulative luminosity functions created using the best fit spectral model to each source with more than 50 source counts in the disc of M31. The cumulative luminosity functions show a distinct flattening in the X-ray luminosity L_X interval $37.0 \lesssim \log L_X \text{ erg s}^{-1} \lesssim 37.5$. Such a feature may also be present in the X-ray populations of several other galaxies, but at a much lower statistical significance. We investigate the number of AGN present in our source list and find that above $L_X \sim 1.4 \times 10^{36} \text{ erg s}^{-1}$ the observed population is statistically dominated by the point source population of M31.

Key words. Galaxies: individual: M31 - X-rays: general - X-rays: binaries

1. Introduction

The Andromeda Galaxy (M31) is the nearest spiral galaxy to our own, lying at a distance of 760 kpc (van den Bergh 2000). The sources in M31 are observed at a nearly uniform distance and through an absorption column significantly lower than for sources in the Galactic plane. Thus M31 is an ideal target for studying the emission from the X-ray point sources in a galaxy similar to the Milky Way.

M31 has been observed with many X-ray observatories since *Einstein*, when van Speybroeck et al. (1979) observed 69 point sources above $5 \times 10^{36} \text{ erg s}^{-1}$. Two ROSAT surveys (Supper et al. 1997, 2001) covered most of the M31 disc and found 560 sources above $5 \times 10^{35} \text{ erg s}^{-1}$. There have also been many *Chandra* (e.g. Williams et al. 2004; Kong et al. 2002, 2003) and XMM-Newton (e.g. Trudolyubov et al. 2006; Pietsch et al. 2005; Osborne et al. 2001; Shirey et al. 2001) surveys of both the disc and central region of M31.

The X-ray emission from M31 is dominated by point sources mostly consisting of X-ray binary systems (XBs). Trudolyubov et al. (2006) surveyed 123 sources in the central region of M31 and reported that the majority have X-ray properties reminiscent of Galactic low mass XBs (LMXBs), and labelled 44 sources as XB candidates based on their spectral properties and variability.

Six neighbouring, slightly overlapping XMM-Newton observations along the major axis of M31 were made in January and June 2002. These observations, along with others taken between 2000 and 2007, form part of a survey of the whole optical D_{25} ellipse of M31. Since the central region of M31 is well studied and the wider survey has not been completed at the time of this

work, we have investigated the five remaining major axis observations that exclude the core region. Henceforth we refer to these fields as the M31 disc fields. These observations were long and uninterrupted; together with the unprecedented effective area of XMM-Newton, they yielded up to 40 times the photon counts of the best previous observations. Previous work on these XMM-Newton fields (see e.g. Pietsch et al. 2005; Trudolyubov et al. 2002) has derived only spectral properties for the brightest few sources.

In this paper we re-analyse the five M31 disc fields. For the first time we extend the spectral analysis to sources down to $L_X \gtrsim 10^{36} \text{ erg s}^{-1}$. We create a new source list, derive the spectral parameters of each source and create spatially resolved cumulative X-ray luminosity functions (CLFs). In Sect. 2 we give details of the observations and data reduction, Sect. 3 covers the analysis and the results of cross correlations with the Pietsch et al. (2005) catalogue and catalogues at other wavelengths. In Sect. 4 we give details of the analysis of our spectral fitting including the creation of CLFs and comments on the contamination of the CLF by background AGN. Finally, Sect. 5 summarises our findings.

2. Observations and Data Reduction

One observation of each disc field of M31 was taken using the EPIC pn (Strüder et al. 2001) and MOS (Turner et al. 2001) cameras on XMM-Newton in January and June 2002; a journal of the observations is presented in Table 1. From north to south, we refer to the fields as North 3, North 2, North 1, South 1 and South 2. Data were processed using XMM-Newton SAS (version 6.5.0) tasks `epproc` and `emproc` with up

to date calibration. There are also multiple observations of the central region taken between 2000 and 2005; these have been analysed by Trudolyubov et al. (2002), Pietsch et al. (2005) and Trudolyubov et al. (2006) and are not covered here.

2.1. Source Detection

For the purposes of source detection, the observations were screened for periods of high background counts in each camera. Lightcurves including all counts above 10 keV were created for each camera, and intervals with levels above 1 count s^{-1} for the pn and 0.5 counts s^{-1} for each of the MOS cameras were excluded. Observations were then synchronised and source detection carried out. For the source detection the data were split into 5 energy bands: (0.2-0.5) keV, (0.5-2) keV, (2-4.5) keV, (4.5-7) keV and (7-12) keV. For the pn data we used only “single” events (PATTERN==0) in the first energy band and for the other bands “singles and doubles” were selected (PATTERN<= 4). Additionally, for the pn, only events with (RAWY> 12) for the pn were used and to avoid emission from the spatially inhomogeneous Copper fluorescent line, the energy range (7.8-8.2) keV was omitted from band 5. For MOS data “singles” to “quadruples” (PATTERN<= 12) were selected. For each camera, source lists were constructed in each energy band using `edetect_chain`¹ with a minimum likelihood threshold of 10. These lists were then combined to form a final source list. All source regions were then set to have a radius of 40'' as this corresponds to $\sim 88\%$ encircled energy at 1.5 keV. Finally the sources in this list were visually inspected for overlapping source regions. When a 40'' source extraction region contained more than one source, the region was reduced to 20''. Any 20'' extraction region containing more than one source was deleted.

2.2. Background Selection

Backgrounds were selected for each source based on the following criteria. Suitable backgrounds must be on the same CCD as the source, have no sources within the background region, and must have a lower count density (fewer counts per unit area) than the source region. The latter criterion ensures that there are no unresolved faint sources or areas of diffuse emission in the background region that combine to an anomalously high count density. For source regions on a chip gap or chip edge background regions must be on the same chip edge or gap and have the same percentage of off-chip area as the source region. Finally, background regions have a radius between one and four times the radius of the source extraction region.

2.3. Scientific Product Extraction

Following Barnard et al. (2007b), synchronised source and background lightcurves with 2.6 s time resolution were extracted from each of the three detectors. These were summed to give a combined, background subtracted EPIC lightcurve for every source.

Energy spectra were extracted from the source and background regions with 5 eV binning for the pn camera and with 15 eV binning for the MOS cameras. A response matrix (RMF) and ancillary response file (ARF) were also generated for each source spectrum. For any source with spectra from both the MOS cameras we added together the two spectra to form a combined MOS spectrum, otherwise just the one MOS spectrum was used

in the following analysis. Counts outside the 0.3-10 keV range were rejected.

3. Analysis

There were 335 point source detections with a minimum likelihood of 10 in the 5 disc fields of M31. These sources are ordered by RA and we present their positions and X-ray properties in Table A.1. Of these 335 detections, 6 sources were detected in two observations and so there are 329 distinct point sources across the disc. Their count rates range from 3.42×10^{-5} to 0.403 counts per second.

3.1. Lightcurves

Lightcurves were binned to 100, 200 and 400 second bins and checked for variability by examining how well they were fit by a line of constant intensity. Sources with a null hypothesis probability of $> 5\%$ in any of the lightcurves were classed as variable. This is a conservative approach that may miss variability in the data, but reduces the number of sources with spurious variability. Around 300 of the M31 disc sources were too faint to detect variability on the timescales sampled. The lightcurves were also visually inspected for bursts, dips or other behaviour. Only source 238 (identified as a flare star by Pietsch et al. 2005 (their source 663) and by Trudolyubov et al. 2005 (their source 22) was found to be variable, with $30 \pm 3\%$ rms variability.

3.2. Energy Spectra

222 of the sources in the disc of M31 have spectra with sufficient photons (>50 source counts in the pn or combined MOS) to allow spectral fitting, the results of which are given in Table A.1.

We binned the pn and MOS spectra depending on source intensity. Spectra exceeding 500 source counts over the observation were grouped to a minimum of 50 counts per bin. Spectra containing between 200 and 499 source counts were grouped to a minimum of 20 counts per bin. Spectra with between 50 and 199 source counts and with more than 50% of the total counts from the source were grouped to a minimum of 10 counts per bin, while those with between 50 and 199 source counts but with less than 50% of the total counts from the source were also grouped to a minimum of 20 counts per bin. Each grouped energy spectrum was freely fit by three spectral models: blackbody, bremsstrahlung and power law emission models, using `xspec 11.3.1`². Sources which have very few or no counts above 2 keV were also fit with a neutron star atmosphere (nsa) model which resembles the emission from a super soft source. For all the models the absorption was a free parameter but with a minimum of at least $0.1 \times 10^{22} \text{ cm}^{-2}$, the Galactic foreground absorption (Dickey & Lockman 1990). The source flux was calculated from the best fit model. The spectral parameters of each source give a greater insight into its properties than its X-ray hardness ratios or variability alone. Sources with less than 50 source counts in both cameras are dealt with on a field by field basis as described below.

3.3. Faint Sources

For the 95 detections with too few photons to allow spectral fitting (< 50 source counts in both cameras), the parameters of

¹ http://xmm.vilspa.esa.es/sas/6.5.0/doc/edetect_chain/index.html

² <http://heasarc.gsfc.nasa.gov/docs/xanadu/xspec/index.html>

Table 1. Journal of XMM-Newton Observations of M31. The field, observation number, date, pointing direction, filter used, total exposure (Exp) and exposure of the good time interval (GTI) and the number of sources detected are given.

Field	Observation	Date	Pointing direction RA/dec (J2000)		Filter	Exp ks	GTI ks	Sources
North 3 (n3)	0109270401	29 June 2002	0:46:38	+42:16:20	Medium	55	46	80
North 2 (n2)	0109270301	26 Jan 2002	0:45:20	+41:56:09	Medium	55	25	57
North 1 (n1)	0109270701	05 Jan 2002	0:44:01	+41:35:57	Medium	55	55	82
South 1 (s1)	0112570201	12 Jan 2002	0:41:25	+40:55:35	Thin	53	44	71
South 2 (s2)	0112570301	24 Jan 2002	0:40:06	+40:35:24	Thin	58	24	45

Table 2. Best fit parameters for power law models applied to the summed spectra of the faint sources in each of the disc fields. We show the total number of faint sources in each field, the power law photon index, Γ , χ^2/dof and for which camera this fit was found. The absorption was fixed to 0.10×10^{22} H atom cm^{-2} for each field. The bracketed numbers are the error in the last significant figure. Where we quote two conversion factors, the first is for the pn camera and the second for the MOS. Errors are unavailable for the best fit power law index to South 1 as the χ^2/dof is > 2 .

Field	Number of faint sources	Γ	χ^2/dof	Camera(s) used	Conversion Factor $\text{erg s}^{-1}/\text{counts s}^{-1}$
North 3	19	2.8(13)	161/122	pn / MOS	$5.71 \times 10^{38} / 9.33 \times 10^{38}$
North 2	32	1.5(4)	39/38	pn / MOS	$3.58 \times 10^{38} / 7.82 \times 10^{38}$
North 1	11	1.00(15)	24/16	MOS	5.73×10^{38}
South 1	16	1.3(-)	450/120	pn	4.75×10^{38}
South 2	17	1.3(4)	56/46	pn	4.54×10^{38}

the best fit absorbed power law for the field were used. First we grouped the spectra according to field and camera (pn or MOS), creating 10 groups. The spectra of the faint sources in each group were then summed to give one spectrum for each camera's observation of every field. The absorption was fixed to 0.1×10^{22} H atoms cm^{-2} and the best fit photon index to the summed spectrum was used to calculate a count rate to flux conversion for that camera's observation of the field. For South 1 we do not quote errors on the photon index because the χ^2/dof is > 2 . Although this is not a good fit to the South 1 sources, it is the best fit power law and so we have used it to maintain consistency across the fields.

Some sources are detected only on the pn or one of the MOS cameras and not in all three. For some fields only one of the two summed spectra (pn or MOS) could be well fit using a power law model. Where a faint source is detected in one camera but a good fit to the summed faint source spectrum for that field is only available for the other camera we do not give a source luminosity.

The parameters of the best fit power law to each field are given in Table 2. For the faint sources the quoted conversion factor was applied to the exposure corrected count rate. There is an obvious change in the photon index in the northern disc: with increasing distance from the centre of M31 the best fit power law becomes softer. However we caution against drawing conclusions from this as it is based on the summed spectrum of a small number of faint sources and the photon indices are consistent with each other within errors.

We have calculated the 0.3-10 keV luminosity from either a source spectrum or from an average model for the relevant field, for 317 of the 329 sources, and these are given in Table A.1.

3.4. Cross-correlations with other M31 catalogues

We searched for cross-correlations within a radius of $3((\sigma_{\text{statistical}})^2 + (\sigma_{\text{systematic}})^2)^{1/2}$, where, for the uncorrected XMM-Newton positions from this survey, $\sigma_{\text{statistical}} = 1''$ and $\sigma_{\text{systematic}} = 3''$. The statistical error is taken from the 2XMM catalogue³. This error is strongly dependent on source counts, however for our range of source count rates we have assumed a representative value of 1 arcsecond for the statistical error. The systematic error is derived from the offset to each field. The most accurate XMM-Newton positions have residual systematic errors of around $0.5''$, and it can be seen from Pietsch et al. (2005) that the M31 disc fields each have an additional offset of $0.3 - 2.3''$. Thus we have used a conservative systematic error of $3''$. This gives a search radius of $10''$. For 295 out of our 329 sources we found a source within the search radius in the Pietsch et al. (2005) catalogue, and a summary of the classifications of these sources as determined in Pietsch et al. (2005) are given in Table 3. Sources are either classed as ‘‘candidates’’ or ‘‘members of’’ each class in Pietsch et al. (2005), but here they are grouped together. The hard class contains all the sources with $\text{HR2-EHR2} > -0.2$ or only HR3 and/or HR4 defined, and no other classification (see Pietsch et al. 2005, for the definitions of hardness ratios HR2, HR3, HR4 and EHR2 and full details).

For the 34 sources not in Pietsch et al. (2005) we searched the following catalogues for counterparts:

(i) *X-ray sources*: the *Einstein* (Trinchieri & Fabbiano 1991), ROSAT/PSPC (Supper et al. 1997, 2001) and *Chandra* (Williams et al. 2004; Kaaret 2002) catalogues.

(ii) *Stellar objects*: USNO-B1 (Monet et al. 2003), 2MASS (Cutri et al. 2003) and the Local Group Survey (Massey et al. 2006).

³ http://xmmssc-www.star.le.ac.uk/Catalogue/UserGuide_xmmcat.html

Table 3. Summary of classifications of our sources from Pietsch et al. (2005).

Type	Number
hard	207
foreground star	42
AGN/Galaxy	19
Supernova remnants	11
Globular cluster source	13
Supersoft source	2
X-ray binary system	1

(iii) *Radio sources:* VLA all sky catalogue (Condon & Kaplan 1998) and catalogue of sources within M31 (Walterbos et al. 1985).

(iv) *Globular cluster candidates:* the Bologna catalogue (Galleti et al. 2004) and the catalogue by Kodaira et al. (2004).

(v) *Supernova remnant candidates:* catalogues by Magnier et al. (1995) and Ford & Jacoby (1978).

Only 2 of the 34 sources in this survey are not found in any other catalogue listed above. Eight sources are identified in either Supper et al. (1997) or Supper et al. (2001), one of which (source 184) is identified as a variable supernova remnant (SNR). Two radio sources were found in Condon & Kaplan (1998) (Sources 184 and 23), both of these are also in the Supper et al. (1997) or Supper et al. (2001) source lists. All the other sources have potential counterparts in the optical catalogues and are classified as <hard> following the convention of Pietsch et al. (2005).

The classification for all 327 sources are given in Table A.1; we distinguish the sources classified in this work by a ⁽¹⁾ beside their classification.

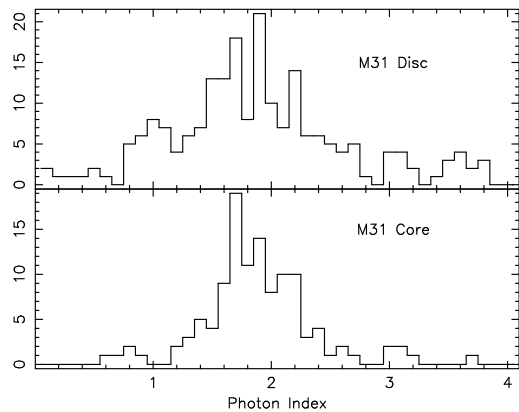
4. Results

We present a summary of the results of our spectral analysis, with the number of detections and faint sources per field as well as a breakdown of the best fit models in each field, in Table 4. The quoted luminosity of the faint limit in Table 4 is the luminosity of the brightest source with less than 50 source counts. Full details of the source positions, spectral fitting and classification (see Sec. 3.4) of each source are listed in Table A.1.

4.1. Spectral Properties

Table 4 shows that a power law model is the best fit model in the majority of cases, although Fig. 1 shows a wide range of best fit photon index. Only four sources with more than 50 source counts have few or no counts above 2keV. These are fit with the nsa model. Of these four only two sources are best fit with the nsa model, accordingly these sources are described as supersoft. Of the three models tested in this survey (see Sec. 3.2) foreground sources would be best fit by a blackbody model; in fact 10 of the 27 sources best fit by a blackbody model in this work are classified as foreground stars in Pietsch et al. (2005) (see Table A.1).

Following the work of Trudolyubov et al. (2006) on the central region of M31, we investigated the distribution of photon index for all sources, not just those for which a power law was the best fit. Figure 1 shows the distribution of the best fit

**Fig. 1.** Distribution of photon index derived from the best fit power law model for each source, with the exception of very soft sources ($\Gamma > 4$). The M31 disc data is shown in the top panel and the data from the central region from Trudolyubov et al. (2006) is shown in the lower panel. The bin width is 0.1.

power law photon index (Γ) to every source. We have compared the data from the disc to sources in the central region from Trudolyubov et al. (2006), who used the same method to derive the spectral indices except that they have presented a weighted mean of the spectral indices derived from multiple observations. There are 33 disc sources with extremely soft spectra ($\Gamma > 4$) which are not plotted.

Figure 1 shows a broad peak in both the central region and the disc fields at $\Gamma \sim 1.7$ which is expected for low mass X-ray binary systems (see Trudolyubov et al. 2006). However the disc sources also show a peak at $\Gamma \sim 1$, a feature which is absent in the central region. While this excess is seen most obviously in the full disc sample, it is also seen in each field individually. The excess is suggestive but a KS test does not rule out that both samples in Fig. 1 are drawn from the same parent population (KS probability 0.36)

There are 23 disc sources with $0.8 \leq \Gamma \leq 1.2$ and seven of these have very large errors to the best fit photon index. The variation in χ^2 around the best fit photon index was investigated for all 23 sources. Five of the seven with large errors were found to have a very shallow variation in χ^2 . This indicates that the best fit Γ is not well defined, we thus exclude these sources from the group with $0.8 \leq \Gamma \leq 1.2$. A photon index of around 1 is expected from magnetically accreting neutron stars (White et al. 1995) and thus indicates the presence of highly magnetic neutron stars in the disc of M31. Since the magnetic field of the neutron star is expected to be weaker in LMXBs than HMXBs (Tauris & van den Heuvel 2006), these sources are strong HMXB candidates - the first such candidates in M31. The 18 HMXB candidates are given in Table 5; we have 16 good candidates with small errors and two secondary candidates with a large 90% confidence interval but a sharply defined minimum. Table 5 gives astrometrically corrected positions from the source catalogue of Pietsch et al. (2005) where available. For the three HMXB candidates not in the source catalogue of Pietsch et al. (2005), we apply the appropriate astrometric corrections as given by Pietsch et al. (2005) to calculate the positions quoted in Table 5. For each of the HMXB candidates we also give the details of the best fit power law model (n_{H} and Γ), the luminosity derived from that fit and the V magnitude extinction, calculated from the X-ray band absorption via $A_v = n_{\text{H}} / (1.79 \times 10^{21}) \text{ cm}^{-2}$, see Predehl & Schmitt (1995). From

Table 4. Overview of the source spectral analysis for each field. “Faint” denotes the number of sources with <50 source counts, in brackets is the number of sources for which we cannot quote a luminosity. For details on the HMXB candidates see text. The faint limit is the luminosity below which all sources have less than 50 source counts.

Field	detections	faint	Number of sources best fit by				HMXB candidates	Luminosity of faint limit, erg s^{-1}
			power law	blackbody	bremsstrahlung	nsa		
North 3	82	19 (3)	55	2	5	0	7	8.6×10^{35}
North 2	57	32 (0)	18	4	3	0	3	1.7×10^{36}
North 1	80	11 (2)	55	8	6	0	3	5.0×10^{35}
South 1	71	16 (5)	41	9	4	1	3	7.4×10^{35}
South 2	45	17 (3)	23	4	0	1	2	9.8×10^{35}

Table 5. X-ray properties of the 18 candidate HMXBs with a photon index between 0.8 and 1.2. Coordinates are astrometrically corrected. The parameters of the best fit power law model are quoted in columns 5 & 6. The symbol f signifies that the absorption was fixed to 0.1×10^{22} H atoms cm^{-2} for that field. 90% confidence interval errors are quoted for both the absorption and photon index. Next we give the luminosity derived from the best fit model, the bracketed numbers are the error in the last significant figure. The luminosity and its errors are calculated from the 90% confidence interval. We also give the V magnitude absorption at the distance of M31. The final column indicates the Massey et al. (2006) designation of any optical source within $3.3''$ of the astrometrically corrected position. The strong candidates are listed in the top section of the table and the secondary candidates in the lower section.

Field	Source Number	RA (J2000)	Dec (J2000)	n_{H} / 10^{22} H atom cm^{-2}	Photon index	Luminosity / 10^{36} erg s^{-1}	A_{V}	Optical coincidence
South 2	21	0:40:01.50	+40:32:45.9	$0.4^{+0.6}_{-0.3}$	$0.9^{+0.4}_{-0.5}$	2.3(10)	2.29	-
South 2	34	0:40:17.07	+40:48:40.7	$0.21^{+0.67}_{-0.14}$	$1.2^{+1.0}_{-0.7}$	8(4)	1.17	-
South 1	99	0:42:10.97	+41:06:47.6	f	$0.8^{+0.5}_{-0.4}$	9(4)	0.56	J004210.83+410647.2
South 1	106	0:42:16.76	+41:00:21.0	$0.4^{+0.6}_{-0.3}$	$1.1^{+0.6}_{-0.4}$	5(2)	2.12	-
North 1	123	0:43:01.44	+41:30:17.5	$0.18^{+0.07}_{-0.06}$	$0.9^{+0.1}_{-0.1}$	74(6)	1.01	J004301.51+413017.5
North 1	149	0:43:54.50	+41:31:04.0	f	$0.9^{+0.7}_{-0.7}$	1.0(7)	0.56	J004354.62+413101.0
North 1	160	0:44:06.64	+41:38:57.8	f	$1.0^{+0.6}_{-0.7}$	1.1(8)	0.56	-
North 1	172	0:44:20.87	+41:35:41.9	f	$1.1^{+0.6}_{-0.6}$	1.3(9)	0.56	J004421.01+413544.3
North 1	197	0:44:47.29	+41:44:12.6	f	$1.0^{+0.8}_{-0.7}$	5(3)	0.56	-
North 2	256	0:45:58.82	+42:04:27.5	$0.3^{+0.4}_{-0.2}$	$1.2^{+0.4}_{-0.5}$	5(2)	1.62	J004558.98+420426.5
North 3	234	0:45:34.96	+42:17:53.0	f	$0.9^{+0.7}_{-0.6}$	4(3)	0.56	J004534.90+421752.8
North 3	236	0:45:37.31	+42:12:33.4	f	$0.9^{+0.6}_{-0.5}$	3(2)	0.56	-
North 3	294	0:46:43.80	+42:09:48.2	f	$1.1^{+0.4}_{-0.3}$	1.9(10)	0.56	J004644.02+420950.0
North 3	295	0:46:42.82	+42:27:16.3	f	$1.1^{+0.7}_{-0.5}$	3(2)	0.56	-
North 3	302	0:46:53.52	+42:19:14.4	f	$0.9^{+0.6}_{-0.7}$	1.1(7)	0.56	J004653.49+421914.4
North 3	305	0:46:58.61	+42:24:15.5	f	$1.1^{+0.8}_{-0.7}$	2.0(14)	0.56	-
South 2	9	0:39:38.77	+40:47:55.9	f	$0.8^{+0.9}_{-0.7}$	5(4)	0.56	-
North 2	226	0:45:26.66	+41:56:35.3	f	$0.9^{+0.9}_{-0.9}$	1.7(13)	0.56	J004526.58+415633.1

the V magnitude extinction it is also possible to calculate the B–V colour excess $E(B-V) = A_{\text{V}}/3.24$.

The most recent complete optical survey of M31 has been the UBVR I Local Group Survey of Massey et al. (2006). This survey consists of UBVR I and various narrow band coverage of the entire optical D_{25} ellipse of M31 down to a limiting magnitude of $V=24.9$. To search for optical counterparts to our 18 HMXB candidates we adapted the criteria for Galactic luminous Be stars from Sabogal et al. (2005). Galactic Be stars have V-band absolute magnitudes between $M_{\text{V}} -6$ and 0, as well as both $-0.4 < B-V < 0.8$ and $-0.35 < V-I < 0.8$ colour restrictions. After correcting these criteria for the distance to M31 (V magnitude $>$

18 and $(B-V) < 0.8$) we searched the catalogue of Massey et al. (2006) for possible counterparts within $3.3''$ of the astrometrically corrected positions. This search radius is calculated as in Sec. 3.4 where, for the astrometrically corrected XMM-Newton positions, $\sigma_{\text{statistical}} = 1''$ and $\sigma_{\text{systematic}} = 0.5''$. Eight of the 16 good HMXB candidates and one of the two secondary candidates have counterparts within this search radii in Massey et al. (2006), four of these have the magnitudes and colours that we would expect for a Be-type star in M31. All potential counterparts are listed in Table 5.

Using the method described below we investigated the possible contamination of this potential HMXB population by back-

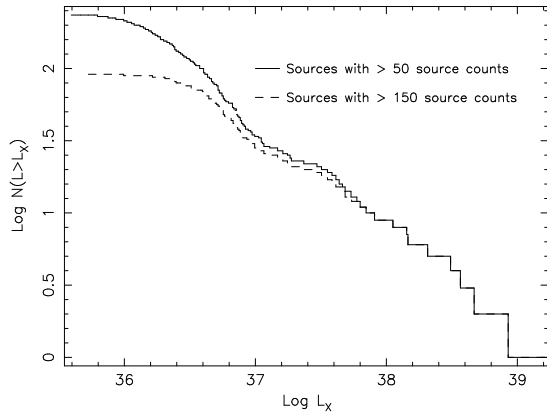


Fig. 3. Cumulative luminosity functions of sources with more than 50 source counts (solid) and of sources with more than 150 source counts (dashed).

ground AGN. We find that AGN could make up $\sim 60\%$ of the total disc population with $L_X > 10^{36}$ erg s $^{-1}$. However Giacconi et al. (2001) found that the average AGN spectrum of sources in the Chandra Deep Field South (CDFS) was softer than the sources considered here. Even the faintest (hardest) group of sources in the CDFS are found to have $\Gamma = 1.35(\pm 0.20)$, which is softer than the interval $0.8 \leq \Gamma \leq 1.2$ we focus on. We conclude that only few, if any, of the HMXB candidates are AGN. All 18 of these sources should be followed up with further optical observations to investigate the nature of the donor star and confirm their status as HMXBs in M31.

4.2. Luminosity Functions

Figure 2 shows the cumulative luminosity functions (CLFs) of each of the disc fields with the 0.3–10 keV luminosity, L_X , plotted on the x-axis and the number of sources with a luminosity higher than L_X on the y-axis. The confirmed foreground star (source 182), AGN (source 27) and background galaxy (source 112) have been removed from the relevant fields, however we have not removed any of the 59 sources which are only classified as foreground or background candidates by Pietsch et al. (2005). The change between freely fit and faint sources in each field occurs between 5×10^{35} erg s $^{-1}$ and 1.7×10^{36} erg s $^{-1}$. The source luminosities below this limit have been calculated using the conversion factor from the summed faint source spectrum (see Table 2).

South 2 and North 2 have the highest luminosity cutoffs of freely fit sources. This is due to these observations having the shortest good time due to background flaring. These regions also have the smallest number of point source detections. South 1 and South 2 have two and three sources respectively with luminosities below 1×10^{35} erg s $^{-1}$, while the other fields only have sources above this limit. South 1, North 1 and North 3 have similar numbers of point source detections and the change between freely modelled sources and faint sources occurs at a similar luminosity.

In Fig. 3 we present the CLF of all the disc sources combined, for sources with more than 50 source counts, and compare it to the CLF of sources with more than 150 source counts. For both these CLFs we have removed the three sources known not to belong to the disc of M31. This comparison is in order to check the validity of results derived from the spectral fitting

of sources with only 50 source counts. Above $\sim 10^{37}$ erg s $^{-1}$ the two functions are almost identical. Using Sherpa⁴, a straight line fit of the CLFs above 10^{36} erg s $^{-1}$ in Fig. 3 gives a slope $\alpha = 0.7$ for the 50 counts case and $\alpha = 0.6$ for the 150 counts case. The flattening of the CLF at $\sim 10^{37}$ erg s $^{-1}$ is clearly apparent in the CLF of sources with more than 150 source counts, hence demonstrating that it is not an artifact of low count rate source fitting.

Previously Williams et al. (2004), using *Chandra*, found that the northern disc had fewer sources above 10^{37} erg s $^{-1}$ than the southern disc. They found 10 sources with luminosities this value in the southern disc and only 5 in the northern disc, while sources with luminosities below this value are more evenly distributed, with 12 in the southern disc and 11 in the northern (numbers from Fig. 11, Williams et al. 2004). We find that South 1 may be over abundant in bright sources with 11 non globular cluster sources above 10^{37} erg s $^{-1}$, while the other fields have somewhat smaller numbers. There are 5 bright non globular cluster sources in North 1, 3 in North 2, 7 in North 3 and 4 in South 2. In total we find 15 non globular cluster sources brighter than 10^{37} erg s $^{-1}$ in the southern disc and 15 in the northern disc. As there are three northern disc fields and two southern the average number of bright sources per field in the southern disc is slightly larger than in the northern disc; however the difference in the number of sources is not as pronounced as that seen by Williams et al. (2004). This difference is consistent with the discussion below relating to the comparison between using individual spectral fitting and using a single simple spectral model as assumed by Williams et al. (2004)

We identify the luminosity below which these observations are incomplete as the luminosity at which we see a break in the CLF of the whole disc, see Fig. 4. This limit is $\sim 1 \times 10^{36}$ erg s $^{-1}$ which is in line with limits quoted in Trudolyubov et al. (2002) (detection limit 5×10^{35} erg s $^{-1}$, completeness limit $\sim 10^{36}$ erg s $^{-1}$ for the central region, North 1 and North 2). *Chandra* surveys (Kong et al. (2003) (detection limit 10^{35} erg s $^{-1}$, completeness limit 10^{36} erg s $^{-1}$) and Williams et al. (2004) (completeness limit 4×10^{36} erg s $^{-1}$ in the disc)) also have similar limits.

The CLF of each field was fit individually with a power law above and below the completeness break $L_b = 1 \times 10^{36}$ erg s $^{-1}$. The results are given in Table 6 (columns 2 & 3 entitled “Freely Fit”). The slopes of the disc CLFs above L_b are between the values expected for starburst galaxies and for spiral galaxies from Kilgard et al. (2002). Given that we are examining the disc of a spiral galaxy, this is to be expected. Fitting the CLF of the bulge of M31, Shirey et al. (2001) find a slope of 1.77 ± 0.35 for $37.4 \leq \log L_X \text{ erg s}^{-1} < 38.1$, flattening to $\alpha = 0.43$ for $\log L_X \text{ erg s}^{-1} < 37.4$. According to the surveys of Colbert et al. (2004) and Kilgard et al. (2002) galaxies with ongoing or recent star formation show flatter CLFs than elliptical galaxies consisting of old populations. Comparing the slope of the bulge CLF from Shirey et al. (2001) with those of the disc from this work (see Table 6) show that the CLF of the disc is flatter than that of the core. This result is consistent with the fact that there is more on-going star formation in the disc of M31 than in the core.

Kilgard et al. (2002) analysed seven spiral and starburst galaxies, not including M31, in a *Chandra* mini-survey. They used an absorbed 5 keV bremsstrahlung emission model to convert from count rate to flux for all detected sources. In order to make a direct comparison between our work and the results from Kilgard et al. (2002), we used a 5 keV thermal bremsstrahlung model with fixed photoelectric absorption ($n_H =$

⁴ <http://cxc.harvard.edu/sherpa/index.html>

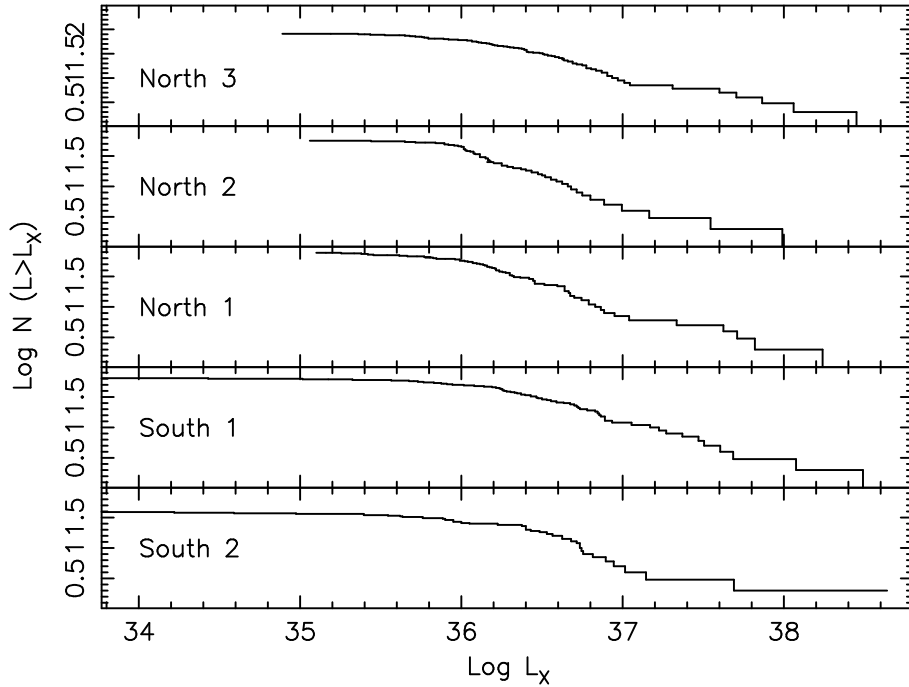


Fig. 2. Cumulative luminosity functions of each of the disc fields. The y-axis range is 0 to 2, except for North 3 where it is 0-2.5.

Table 6. Field by field comparison of the slopes above and below the break luminosity (L_b) for the CLFs created from freely fit spectra and the CLFs of luminosities derived from fixed models. L_b is set to 10^{36} erg s^{-1} , the slopes are for the CLF above and below L_b . Data for the bulge of M31 comes from Shirey et al. (2001) where the break is 2.5×10^{36} erg s^{-1} .

Data	Freely Fit		Fixed Model	
	CLF slope above L_b	CLF slope below L_b	CLF slope above L_b	CLF slope below L_b
North 3	0.7	0.15	0.8	0.4
North 2	0.8	0.12	0.8	0.5
North 1	0.7	0.13	0.8	0.8
South 1	0.7	0.05	1.0	0.2
South 2	0.5	0.06	0.6	0.4
Bulge	1.8(4)	-		

0.1×10^{22} H atom cm^{-2}) to calculate the luminosity of all the M31 disc sources. Figure 5 shows the North 3 CLF obtained in this way, as well as the freely fit CLF. There are two main differences: firstly, fixing the model gave sources which were fainter on the whole than the freely fit sources, and the total luminosity of each field was reduced to only $1 - 3 \times 10^{38}$ erg s^{-1} rather than $4 - 20 \times 10^{38}$ erg s^{-1} . The second effect was the change in average slope of the CLF of each of the fields from $\alpha \approx 0.7$ when the source spectra were freely fit, to $\alpha \approx 0.8$ for the fixed model sources. Kilgard et al. (2002) conclude that steeper slopes of CLFs imply less star formation. We have found that the freely fit CLF was not as steep as the CLF of the fixed model sources and thus the CLF slope-SFR calibration could be systematically offset. A similar finding for NGC 253 is discussed in detail by Barnard et al. (2007a) and Barnard et al. (2008).

Figure 4 shows the CLF of all the disc sources (excluding the 3 identified foreground and background objects), with and without globular cluster (GC) sources. It can be seen that there is a distinct flattening of the CLF in the range $37.0 \leq \log L_x / \text{ergs}^{-1} \leq 37.5$ present in both samples. A KS test shows that the sample with GC sources has a 2.5% chance being drawn

from the same population that is represented by the best fit power law of the data between $36 \leq \log L_x / \text{ergs}^{-1} \leq 38$, while the corresponding probability for the sample without GC sources is 2.1%. The K-S probability becomes larger if a power law fit for the full range of luminosities, including the 8 and 3 sources, respectively, that are brighter than 10^{38} erg s^{-1} , is considered. Although the KS test remains inconclusive we point out that the reality of the flattening in the CLF is supported by the fact that it can also be seen in the CLFs of the M31 disc sources derived from prescribed models (see Fig. 5), in the higher count rate sources only (see Fig. 3) and in some of the individual fields of M31 (especially North 3, North 1 and South 2, see Fig. 2). As well as in the CLF of M31 sources, it is possible that the same feature is also present in the CLFs of the SMC (Shtykovskiy & Gilfanov 2005) and M33 (Grimm et al. 2005) which are both predominantly young populations but have some evidence for a LMXB contribution.

This feature could be due to the emission from a mixture of HMXB and LMXB populations (see Grimm et al. 2002, for work on the sub-populations of the Milky Way) or possibly due to a change in the nature of the compact object. Kalogera (2007)

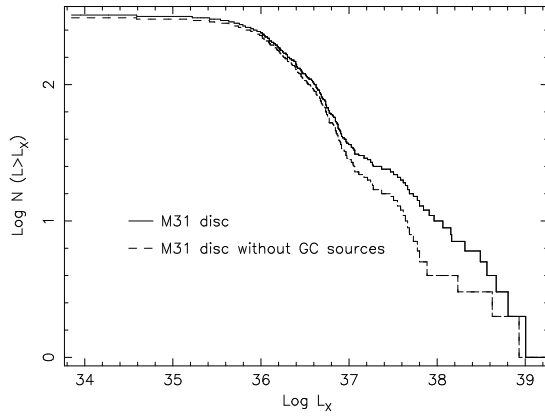


Fig. 4. Cumulative luminosity function of all source in the disc of M31 (solid), compared to the luminosity function of the disc with known globular cluster sources removed (dashed).

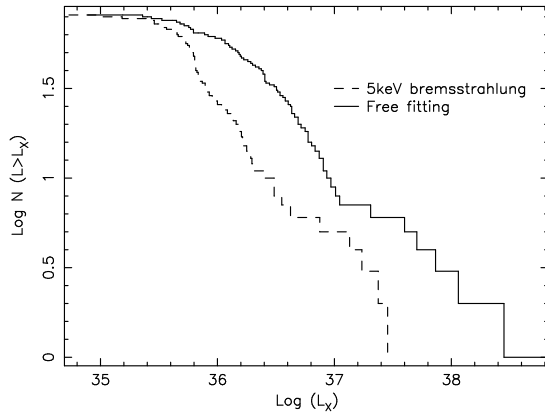


Fig. 5. Cumulative luminosity functions of North 3. The solid line consists of both the freely fit and faint sources from this work, while the dashed line is the luminosity of sources derived from assuming a bremsstrahlung emission model with $kT = 5$ keV (Kilgard et al. 2002).

have reported that they have observed such a dip in theoretical population models, associated with the transition from a binary population with main sequence donors (below $\sim 10^{37}$ erg s^{-1}) to a population with red giant donors (above the dip). This is because, for most magnetic braking laws, the mass transfer rate driven by nuclear expansion of donors (as in red giant donors) is higher than that for mass transfer driven by orbital angular momentum losses (short period systems with main sequence donors). We show in Sec 4.3 below that the flattening is not due to a change in the background AGN CLF.

4.3. AGN Contamination

The CLF for the combined disc flattens below 1×10^{36} erg s^{-1} , while the very faintest sources are around 10^{34} erg s^{-1} . We expect that there is a significant contribution from background AGN at these faint luminosities.

Moretti et al. (2003) consider the AGN contribution in a hard (2-10 keV) and soft (1-2 keV) energy band. We assume a standard AGN spectrum, a power law model with $\Gamma = 1.44$ (following Rosati et al. 2002), to calculate the AGN flux in our 0.3-10 keV band. We calculated the number of background sources

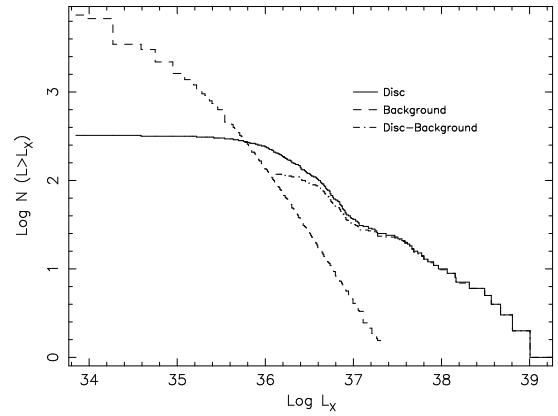


Fig. 6. Cumulative luminosity functions of the population of sources in the disc of M31 from this work (solid) and the derived AGN background (dashed). Also shown for luminosities above 1.4×10^{36} erg s^{-1} is the CLF of the disc with the derived background contribution subtracted (dot-dash).

in each field above the 0.3-10 keV incompleteness limit of $L_X = 10^{36}$ erg s^{-1} (corresponding to a 1-2 keV flux limit of 8.5×10^{-14} erg s^{-1} and a 2-10 keV limit of 1.9×10^{-14} erg s^{-1}). Given that the area of each field is 0.20 deg 2 and using Moretti et al. (2003, Eq. 2) we find that there are 26-30 background sources above 10^{36} erg s^{-1} in each disc field of M31. The lower limit is calculated assuming that all the sources visible in the soft band are also seen in the hard band, the upper limit assumes that none of the sources seen in the soft band are seen in the hard band.

We can then estimate the shape of the CLF intrinsic to the M31 disc by removing the background AGN contribution according to Moretti et al. (2003). In Fig. 6 we show the observed complete disc CLF (Disc), with a total area of 0.98 deg 2 , and the calculated sum of the hard and soft background contributions per 0.98 deg 2 (Background). According to Moretti et al. (2003) the soft sources do not contribute above $\sim 2.8 \times 10^{36}$ erg s^{-1} and so the total background contribution is very close to the number of sources seen in the hard (2-10 keV) band. The upper limit total is shown in Fig. 6 as a dashed line. The model shows that the observations are incomplete below a few $\times 10^{36}$. We also show our estimation of the CLF of sources intrinsic to M31 (Disc CLF with the Background CLF subtracted) only above the luminosity at which there are more sources in the disc than in the background (1.4×10^{36} erg s^{-1}). Below this luminosity the complete M31 CLF is dominated by the background contribution, and the incompleteness of the survey is obvious. We note that the flattening of the CLF near 10^{37} erg s^{-1} is still very prominent in the background corrected CLF.

5. Conclusions

We have revisited five archival XMM-Newton observations of the disc of M31. These data revealed 335 point detections across the 5 fields constituting 329 discrete point sources. All the sources were fit with three spectral models: blackbody, bremsstrahlung and power law and the results of these fits were examined.

Using only the best fit power law model to each source, we investigated the distribution of photon indices of these fits. The broad range of photon index seen in Fig. 1 and the difference in the CLFs seen in Fig. 5 cast doubt on the validity of assuming the same spectral model for all sources when analysing more distant

X-ray point source populations. Individual spectral fitting has identified the first 18 HMXB candidates in the disc. The HMXB candidates are all best fit by a power law with a photon index of 0.8-1.2 indicating magnetically accreting neutron stars.

For the first time X-ray point sources in M31 with as few as 50 source counts have been individually spectrally fit, in contrast to previous surveys which have used the same assumed model for all sources except the very brightest. This has led us to create the first CLFs of the M31 disc region created from 240 individually spectrally fit sources shown in Fig. 2. It can be seen that the CLFs of the fields are quite similar across the disc of M31 and that there are no obvious changes in the CLF slopes with increasing apparent distance from the core. The CLFs of both individual fields (Fig. 2) and the entire disc both with and without GC sources (Fig. 4) show a distinct flattening between $37.0 \leq \log L_X \text{ erg s}^{-1} \leq 37.5$. This flattening could be due to the emission from a mixture of HMXB and LMXB populations or due to a change in the nature of the compact object or the donor star. This prominent flattening in the CLF of M31 sources may also appear at a lower statistical significance in the CLFs of several other galaxies.

Each observation contains not only the point sources in M31 but also some contamination from foreground and background sources. We have estimated that there are around 20-31 background AGN above $10^{36} \text{ erg s}^{-1}$, in each field observed, and find that above $1.4 \times 10^{36} \text{ erg s}^{-1}$ there are few background AGN according to Moretti et al. (2003). The CLF here is dominated by the sources intrinsic to the disc of M31 and any foreground interlopers. Following the correlations of the PSPC ROSAT survey with optical catalogues (Supper et al. 2001), we expect 5-10 foreground objects above $10^{36} \text{ erg s}^{-1}$ for each XMM-Newton field (Shirey et al. 2001).

M31 is a prime target for population surveys because of its proximity and similarity to our own Galaxy. We have investigated the X-ray point sources in the disc of M31 in detail and this population challenges theoretical models to explain the features seen in the distribution of sources and in the CLF.

Acknowledgements. We would like to thank the referee, Sergei Trudolyubov for very helpful comments. We also thank Wolfgang Pietsch and Simon J. Clark for useful conversations during this work. LSG acknowledges support from the Open University. Astronomy research at the Open University is supported by a STFC rolling grant. JPO acknowledges support from STFC.

References

- Barnard, R., Shaw Greening, L., & Kolb, U. 2007a, ArXiv e-prints, 710
 Barnard, R., Shaw Greening, L., & Kolb, U. 2008, MNRAS, in press
 Barnard, R., Trudolyubov, S., Kolb, U. C., et al. 2007b, A&A, in press [astro-ph/0703120]
 Colbert, E. J. M., Heckman, T. M., Ptak, A. F., Strickland, D. K., & Weaver, K. A. 2004, ApJ, 602, 231
 Condon, J. J. & Kaplan, D. L. 1998, ApJS, 117, 361
 Cutri, R. M., Skrutskie, M. F., van Dyk, S., et al. 2003, 2MASS All Sky Catalog of point sources. (The IRSA 2MASS All-Sky Point Source Catalog, NASA/IPAC Infrared Science Archive. <http://irsa.ipac.caltech.edu/applications/Gator/>)
 Dickey, J. M. & Lockman, F. J. 1990, ARA&A, 28, 215
 Ford, H. C. & Jacoby, G. H. 1978, ApJS, 38, 351
 Galletti, S., Federici, L., Bellazzini, M., Fusi Pecci, F., & Macrina, S. 2004, A&A, 416, 917
 Giacconi, R., Rosati, P., Tozzi, P., et al. 2001, ApJ, 551, 624
 Grimm, H.-J., Gilfanov, M., & Sunyaev, R. 2002, A&A, 391, 923
 Grimm, H.-J., McDowell, J., Zezas, A., Kim, D.-W., & Fabbiano, G. 2005, ApJS, 161, 271
 Kaaret, P. 2002, ApJ, 578, 114
 Kilgard, R. E., Kaaret, P., Krauss, M. I., et al. 2002, ApJ, 573, 138
 Kodaira, K., Vanevičius, V., Bridzjus, A., et al. 2004, PASJ, 56, 1025
 Kong, A. K. H., DiStefano, R., Garcia, M. R., & Greiner, J. 2003, ApJ, 585, 298

- Kong, A. K. H., Garcia, M. R., Primini, F. A., et al. 2002, ApJ, 577, 738
 Magnier, E. A., Prins, S., van Paradijs, J., et al. 1995, A&AS, 114, 215
 Massey, P., Olsen, K. A. G., Hodge, P. W., et al. 2006, AJ, 131, 2478
 Monet, D. G., Levine, S. E., Canzian, B., et al. 2003, AJ, 125, 984
 Moretti, A., Campana, S., Lazzati, D., & Tagliaferri, G. 2003, ApJ, 588, 696
 Osborne, J. P., Borozdin, K. N., Trudolyubov, S. P., et al. 2001, A&A, 378, 800
 Pietsch, W., Freyberg, M., & Haberl, F. 2005, A&A, 434, 483
 Predehl, P. & Schmitt, J. H. M. M. 1995, A&A, 293, 889
 Rosati, P., Tozzi, P., Giacconi, R., et al. 2002, ApJ, 566, 667
 Sabogal, B. E., Mennickent, R. E., Pietrzyński, G., & Gieren, W. 2005, MNRAS, 361, 1055
 Shirey, R., Soria, R., Borozdin, K., et al. 2001, A&A, 365, L195
 Shtykovskiy, P. & Gilfanov, M. 2005, MNRAS, 362, 879
 Strüder, L., Briel, U., Dennerl, K., et al. 2001, A&A, 365, L18
 Supper, R., Hasinger, G., Lewin, W. H. G., et al. 2001, A&A, 373, 63
 Supper, R., Hasinger, G., Pietsch, W., et al. 1997, A&A, 317, 328
 Tauris, T. M. & van den Heuvel, E. P. J. 2006, Formation and evolution of compact stellar X-ray sources (Compact stellar X-ray sources), 623–665
 Trinchieri, G. & Fabbiano, G. 1991, ApJ, 382, 82
 Trudolyubov, S., Priedhorsky, W., & Cordova, F. 2006, ArXiv Astrophysics e-prints
 Trudolyubov, S. P., Borozdin, K. N., Priedhorsky, W. C., Mason, K. O., & Cordova, F. A. 2002, ApJ, 571, L17
 Turner, M. J. L., Abbey, A., Arnaud, M., et al. 2001, A&A, 365, L27
 van den Bergh, S. 2000, The Galaxies of the Local Group (The galaxies of the Local Group, by Sidney Van den Bergh. Published by Cambridge, UK: Cambridge University Press, 2000 Cambridge Astrophysics Series, vol no: 35, ISBN: 0521651816.)
 van Speybroeck, L., Epstein, A., Forman, W., et al. 1979, ApJ, 234, L45
 Walterbos, R. A. M., Brinks, E., & Shane, W. W. 1985, A&AS, 61, 451
 White, N. E., Nagase, F., & Parmar, A. N. 1995, in X-ray binaries, p. 1 - 57, 1–57
 Williams, B. F., Garcia, M. R., Kong, A. K. H., et al. 2004, ApJ, 609, 735

Online Material

Appendix A:

In this section we give positional and spectral information on all 335 point source detections in five archival XMM-Newton observations of the disc of M31. Table A.1 gives the source numbers in order of RA and the positions as returned by the source detection routines (i.e. no astrometric corrections were applied). We also provide details of which camera the source spectra or counts are taken from and details of the best fit spectral model for each source, including the absorption (n_{H}), best fit photon index (Γ) or temperature (kT) depending on which model, and the luminosity derived from that fit. The symbol f signifies that the absorption was fixed to $0.1 \times 10^{22} \text{ H atom cm}^{-2}$ for that source. Note that several of the faint sources display a very large formal uncertainty in n_{H} . The actually best fit values were accepted only if they exceeded the Galactic foreground value ($n_{\text{H}} = 0.1 \times 10^{22} \text{ H atom cm}^{-2}$). Errors on the absorption and Γ/kT are the two sided, non-symmetric errors derived by xspec. The luminosity given is the mean value of the 90% confidence interval and hence has symmetric errors quoted in brackets. Best fit values are given for all sources with more than 50 source counts; even for cases where the fit implies significant or very large error bars. Sources with less than 50 source counts are denoted with “faint” as their best fit model, these sources are then summed by field and the parameters of the best fit power law to the summed spectrum applied to each source. Hence for the faint sources no absorption or Γ/kT are given. Finally we give a classification for each source. These are the classifications and source number from Pietsch et al. (2005) where the sources appear in that work. For the 34 sources not in Pietsch et al. (2005) as well as source 238 we give our own classifications and each of these have a ¹ next to it.

Table A.1. Position and spectral properties of each source detected in five archival XMM-Newton observations of the disc of M31. We give the detected source position and detection camera(s) for each source. The best fit model to a source can be faint (less than 50 source counts), pl (power law), bb (blackbody), br (bremsstrahlung), nsa (neutron star atmosphere) or diskbb (disk blackbody). Unless a source is faint we then give the absorption (n_{H}) and appropriate parameter (photon index, Γ , or temperature, kT) of the best fit model. The symbol f signifies that the absorption was fixed to 0.1×10^{22} H atom cm^{-2} for that source. For all sources we then quote the luminosity for that source derived from the model parameters with 90% confidence errors in brackets, and finally a classification, either from Pietsch et al. (2005) with the source number, or this work (denoted with a ¹).

Source	RA (J2000)	Dec (J2000)	Camera	Best Fit Model	n_{H} / 10^{22} cm^{-2}	Γ/kT keV	Luminosity / 10^{36} erg s^{-1}	Classification
1	00 : 38 : 56.5	+ 40 : 34 : 51		faint			-	< hard > 1
2	00 : 38 : 59.9	+ 40 : 39 : 11		faint			0.044	< fgstar > 2
3	00 : 39 : 23.8	+ 40 : 29 : 56	mos	pl	0.3 ^{+3.0} _{-0.3}	1.1 ^{+3.8} _{-1.4}	2.85 (2.01)	< hard > 11
4	00 : 39 : 25.1	+ 40 : 37 : 20		faint			0.300	< hard > ¹
5	00 : 39 : 27.3	+ 40 : 46 : 47		faint			0.008	< hard > 15
6	00 : 39 : 29.0	+ 40 : 35 : 42	pn & mos	pl	0.16 ^{+1.13} _{-0.16}	1.6 ^{+2.3} _{-0.8}	1.23 (0.63) / 1.27 (0.68)	< hard > 18
7	00 : 39 : 31.6	+ 40 : 36 : 16		faint			0.821	< hard > 19
8	00 : 39 : 36.6	+ 40 : 35 : 29		faint			0.767	< hard > 22
9	00 : 39 : 38.7	+ 40 : 47 : 57	pn	pl	f	0.8 ^{+0.9} _{-0.7}	5.40 (3.83)	< hard > 23
10	00 : 39 : 40.3	+ 40 : 35 : 31	pn & mos	pl	0.24 ^{+0.18} _{-0.12}	0.6 ^{+0.2} _{-0.3}	3.87 (0.95) / 3.85 (0.78)	< hard > 24
11	00 : 39 : 43.5	+ 40 : 39 : 44	pn	bb	f	0.21 ^{+0.05} _{-0.04}	1.02 (0.5)	< fgstar > 26
12	00 : 39 : 45.7	+ 40 : 44 : 54	pn	pl	1.9 ^{+8.5} _{-1.9}	1.6 ^{+3.8} _{-1.6}	3.47 (3.19)	< hard > 28
13	00 : 39 : 47.9	+ 40 : 34 : 35		faint			0.816	< AGN > 29
14	00 : 39 : 48.9	+ 40 : 35 : 14	pn & mos	pl	0.7 ^{+0.4} _{-0.2}	2.3 ^{+0.7} _{-0.5}	3.32 (1.21) / 3.19 (1.05)	< hard > 30
15	00 : 39 : 56.3	+ 40 : 41 : 00	pn & mos	nsa	1.07 ^{+0.2} _{-0.17}	5.36 ^{+0.02} _{-0.03}	1350 (1020) / 1250 (910)	< fgstar > 31
16	00 : 39 : 57.9	+ 40 : 27 : 26	pn	bb	0.26 ^{+0.16} _{-0.22}	0.13 ^{+0.06} _{-0.02}	5.57 (3.23)	< SNR > 32
17	00 : 39 : 59.7	+ 40 : 31 : 59	pn & mos	pl	0.28 ^{+0.08} _{-0.04}	2.3 ^{+0.2} _{-0.2}	17.0 (3.1) / 19.4 (2.2)	< hard > 33
18	00 : 40 : 00.5	+ 40 : 26 : 41		faint			0.202	< hard > ¹
19	00 : 40 : 01.1	+ 40 : 25 : 24	pn	pl	f	1.2 ^{+0.6} _{-0.5}	2.59 (1.56)	< hard > 34
20	00 : 40 : 01.4	+ 40 : 33 : 23	pn	pl	0.9 ^{+0.9} _{-0.4}	3.2 ^{+2.3} _{-1.0}	4.60 (3.29)	< hard > 36

Table A.1. continued.

Source	RA (J2000)	Dec (J2000)	Camera	Best Fit Model	n_{H} / 10^{22} cm $^{-2}$	Γ/kT keV	Luminosity / 10^{36} erg s $^{-1}$	Classification
21	00 : 40 : 01.6	+ 40 : 32 : 43	pn & mos	pl	0.4 $^{+0.6}_{-0.3}$	0.9 $^{+0.4}_{-0.6}$	2.27 (0.97) / 2.66 (1.12)	< hard > 35
22	00 : 40 : 06.1	+ 40 : 24 : 09		faint			-	< hard > 37
23	00 : 40 : 06.6	+ 40 : 21 : 48		faint			-	SNR 1
24	00 : 40 : 07.1	+ 40 : 41 : 42		faint			0.783	< hard > 40
25	00 : 40 : 07.5	+ 40 : 31 : 14	pn & mos	pl	0.28 $^{+0.52}_{-0.12}$	3.2 $^{+3.3}_{-1.3}$	2.43 (1.63) / 1.68 (1.13)	< fgstar > 42
26	00 : 40 : 08.6	+ 40 : 47 : 12		faint			-	< hard > 43
27	00 : 40 : 13.8	+ 40 : 50 : 06	pn	pl	0.41 $^{+0.02}_{-0.02}$	1.88 $^{+0.05}_{-0.05}$	753 (23)	AGN50
28	00 : 40 : 13.9	+ 40 : 35 : 33	pn & mos	bb	0.7 $^{+0.4}_{-0.6}$	0.1 $^{+0.1}_{-0.04}$	7.36 (7.35) / 7.78 (7.75)	< fgstar > 49
29	00 : 40 : 14.3	+ 40 : 51 : 35		faint			-	< hard > 1
30	00 : 40 : 14.3	+ 40 : 33 : 41	pn & mos	pl	0.16 $^{+0.09}_{-0.05}$	1.38 $^{+0.13}_{-0.14}$	9.25 (1.26) / 9.47 (1.17)	< hard > 51
31	00 : 40 : 16.7	+ 40 : 53 : 07		faint			-	< hard > 53
32	00 : 40 : 16.8	+ 40 : 50 : 37	pn	pl	1.0 $^{+2.3}_{-1.0}$	1.7 $^{+2.4}_{-1.5}$	5.38 (3.95)	< hard > 1
33	00 : 40 : 17.8	+ 40 : 32 : 57	pn	pl	0.3 $^{+3.8}_{-0.2}$	2.0 $^{+8.0}_{-1.1}$	0.98 (0.56)	< hard > 54
34	00 : 40 : 18.2	+ 40 : 48 : 41	pn & mos	pl	0.20 $^{+0.38}_{-0.15}$	1.2 $^{+0.7}_{-0.5}$	8.39 (3.87) / 7.35 (2.66)	< hard > 1
35	00 : 40 : 20.2	+ 40 : 43 : 59	pn & mos	pl	0.16 $^{+0.02}_{-0.02}$	1.58 $^{+0.06}_{-0.06}$	140 (15) / 225 (12)	GIC55
36	00 : 40 : 20.9	+ 40 : 39 : 18	pn & mos	pl	0.8 $^{+1.3}_{-2.4}$	2 $^{+3}_{-1}$	2.44 (1.55) / 2.44 (1.66)	< hard > 56
37	00 : 40 : 22.6	+ 40 : 36 : 09	pn & mos	pl	0.25 $^{+0.12}_{-0.15}$	2.1 $^{+0.3}_{-0.4}$	5.05 (1.49) / 6.17 (1.14)	< hard > 58
38	00 : 40 : 23.6	+ 40 : 53 : 05	mos	bb	f	0.20 $^{+0.07}_{-0.06}$	0.79 (0.56)	< fgstar > 59
39	00 : 40 : 24.1	+ 40 : 29 : 45	pn & mos	pl	0.16 $^{+0.08}_{-0.07}$	1.7 $^{+0.2}_{-0.2}$	11.6 (1.6) / 12.6 (1.4)	< hard > 60
40	00 : 40 : 27.6	+ 40 : 46 : 34		faint			0.407	< hard > 65
41	00 : 40 : 29.5	+ 40 : 37 : 06	pn & mos	pl	0.8 $^{+1.6}_{-0.7}$	3 $^{+2}_{-1}$	2.43 (1.61) / 3.23 (2.33)	< hard > 66
42	00 : 40 : 31.6	+ 40 : 58 : 34		faint			0.153	< SNR > 70
43	00 : 40 : 32.6	+ 41 : 00 : 45		faint			-	< hard > 71
44	00 : 40 : 33.2	+ 40 : 49 : 39	pn	pl	0.3 $^{+1.7}_{-0.3}$	1.4 $^{+4.1}_{-1.2}$	2.08 (1.30)	< hard > 72
45	00 : 40 : 37.7	+ 40 : 40 : 45		faint			-	< SSS > 75
46	00 : 40 : 39.6	+ 41 : 06 : 10	mos	bb	0.6 $^{+2.7}_{-0.6}$	1.6 $^{+0.4}_{-0.3}$	1.58 (1.55)	< hard > 77
47	00 : 40 : 40.0	+ 40 : 25 : 47		faint			0.431	< hard > 78

Table A.1. continued.

Source	RA (J2000)	Dec (J2000)	Camera	Best Fit Model	n_{H} / 10^{22} cm^{-2}	Γ/kT keV	Luminosity / $10^{36} \text{ erg s}^{-1}$	Classification
48	00 : 40 : 42.9	+ 40 : 32 : 41	pn & mos	pl	$0.6^{+0.6}_{-0.3}$	$2.7^{+1.5}_{-0.7}$	5.44 (2.69) / 5.83 (2.83)	< hard > 81
49	00 : 40 : 44.3	+ 40 : 48 : 58	pn & mos	pl	$0.7^{+0.7}_{-0.2}$	$1.5^{+0.7}_{-0.4}$	3.71 (1.06) / 4.14 (1.04)	< hard > 84
50	00 : 40 : 45.4	+ 40 : 51 : 37	pn & mos	bb	f	$0.18^{+0.03}_{-0.02}$	0.75 (0.37) / 0.85 (0.43)	< hard > 88
51	00 : 40 : 46.8	+ 40 : 29 : 12		faint			0.441	< fgstar > 90
52	00 : 40 : 47.1	+ 40 : 55 : 20	pn & mos	pl	$0.32^{+0.18}_{-0.18}$	$2.2^{+0.8}_{-0.6}$	1.86 (0.67) / 1.45 (0.510)	SNR91
53	00 : 40 : 48.1	+ 40 : 51 : 11	pn	pl	f	$2.7^{+1.8}_{-1.6}$	1.95 (1.43)	< hard > 92
54	00 : 40 : 48.8	+ 40 : 49 : 25	mos	br	f	$0.36^{+0.23}_{-0.11}$	1.27 (1.00)	< hard > 94
55	00 : 40 : 48.9	+ 40 : 30 : 33	pn & mos	pl	$0.41^{+0.33}_{-0.18}$	$2.1^{+0.8}_{-0.5}$	5.70 (1.87) / 3.09 (1.86)	< hard > 93
56	00 : 40 : 50.0	+ 41 : 07 : 30		faint			0.495	< hard > 96
57	00 : 40 : 52.7	+ 40 : 36 : 21		faint			0.035	< hard > 98
58	00 : 40 : 56.9	+ 40 : 56 : 38	pn & mos	pl	$0.29^{+0.13}_{-0.12}$	$2.2^{+0.7}_{-0.5}$	1.78 (0.56) / 2.02 (0.52)	< fgstar > 101
59	00 : 41 : 00.3	+ 41 : 00 : 26		faint			0.072	< hard > 105
60	00 : 41 : 06.4	+ 40 : 27 : 08	mos	bb	f	$0.49^{+0.15}_{-0.11}$	3.86 (2.09)	< hard > 108
61	00 : 41 : 07.6	+ 40 : 50 : 47	pn	pl	$0.3^{+2.5}_{-0.3}$	$1.1^{+3.9}_{-0.7}$	1.83 (1.33)	< hard > 111
62	00 : 41 : 08.4	+ 40 : 51 : 28	pn & mos	pl	$0.20^{+0.13}_{-0.09}$	$1.6^{+0.3}_{-0.2}$	7.18 (1.63) / 7.53 (1.12)	< hard > 113
63	00 : 41 : 09.9	+ 41 : 04 : 52	pn & mos	pl	$2.9^{+2.1}_{-1.3}$	$2.6^{+1.3}_{-0.5}$	5.24 (3.9) / 4.85 (3.25)	< hard > 115
64	00 : 41 : 11.8	+ 40 : 54 : 20	mos	bb	f	$0.7^{+0.2}_{-0.2}$	0.74 (0.56)	< hard > 117
65	00 : 41 : 13.0	+ 40 : 51 : 33		faint			-	< hard > 118
66	00 : 41 : 13.2	+ 40 : 59 : 47	pn & mos	pl	$0.15^{+0.04}_{-0.05}$	$2.18^{+0.16}_{-0.11}$	7.12 (1.07) / 7.73 (0.82)	< hard > 119
67	00 : 41 : 14.3	+ 41 : 09 : 05		faint			0.549	< hard > ¹
68	00 : 41 : 15.1	+ 41 : 01 : 00	pn & mos	br	$0.39^{+0.03}_{-0.07}$	$0.27^{+0.04}_{-0.04}$	47.5 (13.7) / 43.9 (13.8)	< hard > 122
69	00 : 41 : 18.1	+ 41 : 06 : 43	pn & mos	pl	$0.21^{+0.10}_{-0.14}$	$2.2^{+0.5}_{-0.4}$	1.74 (0.52) / 1.71 (0.44)	< hard > 125
70	00 : 41 : 18.5	+ 40 : 51 : 58	pn & mos	pl	$0.13^{+0.23}_{-0.13}$	$1.2^{+0.3}_{-0.5}$	2.89 (2.02) / 3.91 (2.10)	< fgstar > 128
71	00 : 41 : 19.6	+ 41 : 00 : 09		faint			0.147	< hard > 130
72	00 : 41 : 21.0	+ 41 : 03 : 39	pn	pl	$0.7^{+3.5}_{-0.7}$	$1.6^{+8.4}_{-2.1}$	0.93 (0.75)	< hard > 132
73	00 : 41 : 21.5	+ 41 : 07 : 54	pn & mos	pl	$0.17^{+0.02}_{-0.02}$	$1.65^{+0.07}_{-0.07}$	30.1 (1.98) / 31.0 (1.62)	< hard > 134
74	00 : 41 : 25.2	+ 40 : 51 : 11	pn & mos	pl	f	$2.07^{+0.09}_{-0.09}$	7.36 (0.88) / 7.93 (0.70)	< hard > 140

Table A.1. continued.

Source	RA (J2000)	Dec (J2000)	Camera	Best Fit Model	n_{H} / 10^{22} cm^{-2}	Γ/kT keV	Luminosity / $10^{36} \text{ erg s}^{-1}$	Classification
75	00 : 41 : 25.6	+ 40 : 58 : 44	pn & mos	pl	$0.5^{+0.5}_{-0.3}$	$1.5^{+0.6}_{-0.4}$	2.51 (0.79) / 2.48 (0.73)	< hard > 141
76	00 : 41 : 26.1	+ 40 : 53 : 25	pn & mos	pl	$0.12^{+0.06}_{-0.06}$	$1.7^{+0.2}_{-0.2}$	8.12 (1.44) / 7.97 (1.08)	< hard > 142
77	00 : 41 : 28.5	+ 40 : 54 : 51		faint			0.615	< hard > 144
78	00 : 41 : 28.8	+ 41 : 02 : 08	pn	nsa	0.28	5.96	0.84 (0.84)	< hard > 145
79	00 : 41 : 31.2	+ 40 : 59 : 57	pn & mos	pl	f	$2.32^{+0.17}_{-0.16}$	3.33 (0.74) / 3.74 (0.61)	< hard > 147
80	00 : 41 : 35.5	+ 41 : 06 : 53	pn & mos	pl	$0.14^{+0.05}_{-0.06}$	$1.92^{+0.16}_{-0.19}$	6.63 (1.17) / 6.97 (1.00)	SNR154
81	00 : 41 : 36.4	+ 41 : 00 : 18	pn & mos	pl	$0.17^{+0.17}_{-0.13}$	$1.6^{+0.3}_{-0.4}$	3.00 (0.97) / 2.50 (0.69)	< fgstar > 157
82	00 : 41 : 37.7	+ 41 : 01 : 07	pn & mos	bb	$1.00^{+0.07}_{-0.30}$	$0.08^{+0.02}_{-0.01}$	328 (305) / 515 (474)	< hard > 159
83	00 : 41 : 41.0	+ 41 : 03 : 33		faint			-	< AGN > 164
84	00 : 41 : 41.8	+ 41 : 00 : 15		faint			-	< hard > 167
85	00 : 41 : 43.2	+ 41 : 05 : 05	mos	pl	$0.17^{+0.22}_{-0.17}$	$1.9^{+0.8}_{-0.6}$	4.11 (0.14)	< fgstar > 168
86	00 : 41 : 45.8	+ 40 : 43 : 04		faint			0.456	< SNR > ¹
87	00 : 41 : 48.3	+ 41 : 07 : 06		faint			0.525	< hard > 174
88	00 : 41 : 49.6	+ 41 : 01 : 07	mos	pl	$0.4^{+1.6}_{-0.4}$	$1.6^{+2.0}_{-0.9}$	1.16 (0.73)	< hard > 175
89	00 : 41 : 51.8	+ 40 : 54 : 28	pn & mos	nsa	f	$5.22^{+0.04}_{-0.06}$	5.48 (4.14) / 8.00 (6.04)	< hard > 185
90	00 : 41 : 52.9	+ 40 : 47 : 09	mos	pl	$0.5^{+0.8}_{-0.5}$	$1.8^{+2.1}_{-1.1}$	1.69 (0.99)	GIC187
91	00 : 41 : 53.4	+ 40 : 53 : 21	pn & mos	pl	$0.14^{+0.04}_{-0.04}$	$2.1^{+0.2}_{-0.2}$	14.2 (1.71) / 15.5 (1.49)	< hard > 190
92	00 : 41 : 53.9	+ 41 : 07 : 24	pn & mos	pl	f	$2.2^{+0.3}_{-0.2}$	6.98 (1.38) / 6.31 (1.17)	< SSS > 191
93	00 : 41 : 56.5	+ 40 : 47 : 13	pn & mos	pl	$0.4^{+0.1}_{-0.1}$	$1.7^{+0.3}_{-0.2}$	15.5 (3.62) / 16.1 (2.02)	< hard > 194
94	00 : 42 : 02.9	+ 40 : 46 : 06	pn & mos	pl	$0.1^{+0.1}_{-0.1}$	$2.0^{+0.6}_{-0.6}$	7.41 (2.51) / 9.63 (2.05)	< hard > 199
95	00 : 42 : 05.9	+ 41 : 02 : 48	mos	bb	$0.5^{+2.9}_{-0.5}$	$0.9^{+0.5}_{-0.3}$	1.53 (1.47)	< GIC > 207
96	00 : 42 : 06.8	+ 41 : 00 : 16	pn	pl	f	$0.8^{+0.5}_{-0.4}$	9.19 (4.35)	< GIC > 208
97	00 : 42 : 07.6	+ 41 : 04 : 36	pn & mos	pl	$0.17^{+0.12}_{-0.13}$	$2.0^{+0.5}_{-0.3}$	2.44 (0.66) / 3.00 (0.69)	< hard > 213
98	00 : 42 : 09.8	+ 40 : 50 : 38	pn & mos	pl	$0.48^{+0.04}_{-0.03}$	$1.46^{+0.06}_{-0.06}$	288 (17) / 284 (11)	< hard > 222
99	00 : 42 : 10.8	+ 41 : 06 : 46	pn	bb	f	$1.8^{+3.7}_{-0.9}$	1.76 (1.49)	< hard > 225
100	00 : 42 : 11.8	+ 40 : 53 : 37		faint			0.010	< hard > 229
101	00 : 42 : 15.6	+ 41 : 01 : 14	pn & mos	pl	$0.27^{+0.04}_{-0.04}$	$2.44^{+0.13}_{-0.14}$	28.6 (2.55) / 30.5 (2.39)	GIC239

Table A.1. continued.

Source	RA (J2000)	Dec (J2000)	Camera	Best Fit Model	n_{H} / 10^{22} cm^{-2}	Γ/kT keV	Luminosity / $10^{36} \text{ erg s}^{-1}$	Classification
102	00 : 42 : 15.8	+ 40 : 59 : 59	mos	pl	$1.6^{+3.5}_{-1.6}$	3^{+4}_{-2}	3.48 (3.10)	< hard > ¹
103	00 : 42 : 16.3	+ 40 : 48 : 15	pn & mos	pl	$0.4^{+0.6}_{-0.3}$	$1.1^{+0.6}_{-0.4}$	4.53 (1.55) / 5.09 (1.58)	< SNR > 242
104	00 : 42 : 16.4	+ 40 : 55 : 52	pn & mos	pl	$0.13^{+0.03}_{-0.03}$	$1.75^{+0.11}_{-0.11}$	33.5 (2.71) / 31.6 (2.25)	< hard > 241
105	00 : 42 : 16.5	+ 40 : 52 : 41	pn	pl	f	3^{+4}_{-2}	2.19 (1.67)	< hard > 243
106	00 : 42 : 18.9	+ 41 : 00 : 23	pn & mos	br	$0.5^{+0.5}_{-0.2}$	$1.5^{+1.4}_{-0.9}$	2.54 (1.12) / 1.92 (0.80)	< hard > ¹
107	00 : 42 : 22.0	+ 40 : 59 : 23	pn	pl	$0.19^{+0.04}_{-0.03}$	$2.5^{+0.2}_{-0.2}$	48.8 (3.87)	< hard > 254
108	00 : 42 : 23.2	+ 41 : 07 : 35	pn	pl	f	$1.5^{+0.3}_{-0.3}$	5.18 (1.93)	< hard > 258
109	00 : 42 : 24.7	+ 40 : 57 : 20	pn & mos	br	f	$5.6^{+1.8}_{-1.2}$	19.2 (2.7) / 20.8 (2.5)	GIC261
110	00 : 42 : 26.0	+ 40 : 54 : 52	pn	pl	$0.21^{+0.07}_{-0.07}$	$2.3^{+0.3}_{-0.3}$	18.0 (2.42)	< hard > 265
111	00 : 42 : 28.7	+ 41 : 04 : 36	mos	bb	f	$0.9^{+0.6}_{-0.3}$	2.24 (2.24)	< hard > 271
112	00 : 42 : 32.9	+ 41 : 03 : 28	pn	pl	f	$1.78^{+0.06}_{-0.05}$	95.7 (6.00)	GIC282
113	00 : 42 : 34.7	+ 40 : 57 : 19	pn & mos	pl	$0.7^{+0.7}_{-0.2}$	$2.2^{+1.3}_{-0.4}$	2.98 (1.28) / 4.05 (1.67)	< hard > 288
114	00 : 42 : 34.9	+ 40 : 48 : 40	pn & mos	pl	3^{+3}_{-2}	$2.0^{+1.3}_{-0.4}$	5.42 (2.41) / 5.32 (2.57)	< hard > 289
115	00 : 42 : 36.2	+ 40 : 58 : 48	pn & mos	pl	$0.20^{+0.16}_{-0.05}$	$1.5^{+0.3}_{-0.2}$	4.91 (1.14) / 4.26 (0.68)	< hard > 293
116	00 : 42 : 42.3	+ 40 : 51 : 50		faint			0.298	Gal315
117	00 : 42 : 51.2	+ 41 : 32 : 12	mos	pl	$0.5^{+0.6}_{-0.5}$	$1.9^{+1.1}_{-0.8}$	4.13 (1.75)	< hard > ¹
118	00 : 42 : 51.8	+ 41 : 31 : 10	mos	br	$0.23^{+0.01}_{-0.01}$	11^{+2}_{-1}	411 (14)	GIC351
119	00 : 42 : 53.4	+ 41 : 29 : 54	mos	pl	$0.13^{+0.25}_{-0.13}$	$1.4^{+0.4}_{-0.4}$	6.48 (1.63)	< hard > 355
120	00 : 42 : 57.7	+ 41 : 39 : 13		faint			0.269	< hard > 363
121	00 : 42 : 58.8	+ 41 : 37 : 33	pn	bb	$0.4^{+1.1}_{-0.4}$	$0.5^{+0.2}_{-0.2}$	1.07 (0.76)	< hard > 367
122	00 : 42 : 59.4	+ 41 : 29 : 45	mos	pl	$0.4^{+0.4}_{-0.2}$	$1.9^{+0.7}_{-0.4}$	5.21 (1.54)	< hard > 370
123	00 : 43 : 01.4	+ 41 : 30 : 18	mos	pl	$0.18^{+0.07}_{-0.06}$	$0.87^{+0.10}_{-0.06}$	73.5 (6.00)	GIC377
124	00 : 43 : 03.8	+ 41 : 38 : 46	pn & mos	pl	$0.18^{+0.22}_{-0.16}$	$1.9^{+0.4}_{-0.6}$	1.83 (0.77) / 2.09 (0.69)	< AGN > 387
125	00 : 43 : 05.2	+ 41 : 40 : 24		faint			0.222	< fgstar > 389
126	00 : 43 : 06.7	+ 41 : 35 : 23	pn	pl	f	$2.5^{+1.2}_{-0.9}$	0.88 (0.69)	< hard > 393
127	00 : 43 : 08.2	+ 41 : 46 : 03	pn	pl	$0.5^{+0.8}_{-0.2}$	$1.8^{+1.2}_{-0.8}$	2.83 (1.15)	< hard > 400
128	00 : 43 : 08.6	+ 41 : 32 : 13	pn	br	f	0.4	0.95 (0.9)	< hard > 402

Table A.1. continued.

Source	RA (J2000)	Dec (J2000)	Camera	Best Fit Model	n_{H} / 10^{22} cm $^{-2}$	Γ/kT keV	Luminosity / 10^{36} erg s $^{-1}$	Classification
129	00 : 43 : 10.4	+ 41 : 38 : 54	pn	pl	5^{+46}_{-5}	$1.9^{+8.1}_{-2.2}$	2.05 (1.91)	< hard > 407
130	00 : 43 : 17.9	+ 41 : 39 : 16	pn & mos	pl	$0.4^{+0.6}_{-0.3}$	$1.5^{+0.9}_{-0.7}$	2.09 (0.93) / 2.33 (0.98)	< hard > 425
131	00 : 43 : 18.6	+ 41 : 43 : 14	pn	br	$0.23^{+0.47}_{-0.15}$	$1.1^{+1.0}_{-0.6}$	0.68 (0.67)	< fgstar > 429
132	00 : 43 : 23.4	+ 41 : 31 : 47	pn & mos	pl	f	$1.8^{+0.4}_{-0.4}$	1.35 (0.74) / 1.51 (0.69)	< hard > 441
133	00 : 43 : 24.9	+ 41 : 35 : 56	pn & mos	pl	f	$1.5^{+0.4}_{-0.4}$	1.41 (0.56) / 1.12 (0.49)	< hard > 444
134	00 : 43 : 25.4	+ 41 : 36 : 52	pn & mos	pl	$0.38^{+0.29}_{-0.18}$	$2.3^{+0.4}_{-0.5}$	1.37 (0.49) / 1.25 (0.41)	< hard > 445
135	00 : 43 : 31.2	+ 41 : 40 : 49	pn & mos	pl	f	$1.9^{+1.0}_{-0.7}$	0.56 (0.44) / 0.94 (0.69)	< hard > 460
136	00 : 43 : 31.6	+ 41 : 45 : 50	pn & mos	pl	$0.8^{+2.3}_{-0.8}$	$1.1^{+2.1}_{-1.1}$	1.96 (1.41) / 1.94 (1.58)	< hard > 462
137	00 : 43 : 35.7	+ 41 : 33 : 22	pn & mos	pl	$0.5^{+0.7}_{-0.3}$	$1.3^{+0.8}_{-0.5}$	1.23 (0.51) / 1.41 (0.56)	< hard > 468
138	00 : 43 : 39.0	+ 41 : 26 : 54	pn & mos	bb	f	$1.33^{+0.01}_{-0.01}$	3.74 (.081) / 3.89 (0.75)	SNR475
139	00 : 43 : 40.5	+ 41 : 41 : 05	pn & mos	pl	$1.7^{+3.8}_{-1.1}$	$2.4^{+2.7}_{-1.0}$	1.57 (1.11) / 1.81 (1.25)	< AGN > 477
140	00 : 43 : 41.5	+ 41 : 42 : 26	pn	bb	f	$0.16^{+0.03}_{-0.02}$	0.62 (0.30)	< fgstar > 479
141	00 : 43 : 42.7	+ 41 : 33 : 11		13060			0.422	< hard > 482
142	00 : 43 : 43.9	+ 41 : 28 : 47	pn & mos	pl	$0.30^{+0.17}_{-0.08}$	$1.7^{+0.3}_{-0.2}$	7.14 (1.09) / 4.66 (0.86)	< GIC > 483
143	00 : 43 : 45.5	+ 41 : 36 : 57	pn & mos	pl	f	$1.84^{+0.16}_{-0.15}$	4.16 (1.31) / 5.08 (1.00)	GIC488
144	00 : 43 : 45.5	+ 41 : 27 : 09	pn	pl	$0.5^{+0.9}_{-0.5}$	$2.0^{+2.5}_{-1.1}$	1.12 (0.59)	< hard > 489
145	00 : 43 : 46.8	+ 41 : 38 : 40	mos	br	f	$0.4^{+0.5}_{-0.2}$	0.62 (0.54)	< fgstar > 492
146	00 : 43 : 47.1	+ 41 : 27 : 47	pn & mos	bb	$0.20^{+0.15}_{-0.06}$	$0.17^{+0.03}_{-0.03}$	2.86 (0.58) / 3.07 (0.58)	< fgstar > 493
147	00 : 43 : 47.2	+ 41 : 33 : 20	pn & mos	pl	$0.5^{+0.8}_{-0.4}$	$1.5^{+0.8}_{-0.5}$	0.95 (0.40) / 1.15 (0.47)	< hard > 494
148	00 : 43 : 48.1	+ 41 : 35 : 34		faint			0.304	< hard > 496
149	00 : 43 : 53.9	+ 41 : 31 : 05	mos	pl	f	$0.9^{+0.7}_{-0.7}$	1.01 (0.73)	< hard > 505
150	00 : 43 : 55.2	+ 41 : 32 : 54	pn	pl	$0.3^{+4.6}_{-0.3}$	3^{+7}_{-6}	1.03 (0.95)	< hard > 506
151	00 : 43 : 56.1	+ 41 : 22 : 04	mos	pl	$0.20^{+0.16}_{-0.17}$	$2.1^{+0.8}_{-0.5}$	4.13 (1.06)	GIC508
152	00 : 43 : 56.6	+ 41 : 49 : 40		faint			-	< hard > ¹
153	00 : 43 : 57.5	+ 41 : 43 : 48	mos	pl	$0.5^{+0.9}_{-0.3}$	$2.1^{+1.3}_{-0.9}$	1.93 (0.88)	< fgstar > 513
154	00 : 43 : 57.5	+ 41 : 30 : 57	pn & mos	pl	f	$1.63^{+0.12}_{-0.11}$	4.68 (0.75) / 4.72 (0.60)	< hard > 512
155	00 : 44 : 00.5	+ 41 : 28 : 03	mos	pl	f	$1.3^{+0.7}_{-0.6}$	1.63 (1.12)	< hard > 515

Table A.1. continued.

Source	RA (J2000)	Dec (J2000)	Camera	Best Fit Model	n_{H} / 10^{22} cm $^{-2}$	Γ/kT keV	Luminosity / 10^{36} erg s $^{-1}$	Classification
156	00 : 44 : 01.8	+ 41 : 40 : 30	pn	pl	0.6 $^{+0.9}_{-0.4}$	3.1 $^{+2.3}_{-1.1}$	1.63 (1.00)	< hard > 517
157	00 : 44 : 02.7	+ 41 : 39 : 28	pn & mos	pl	0.9 $^{+0.3}_{-0.2}$	3.1 $^{+0.5}_{-0.4}$	5.90 (2.36) / 5.26 (1.69)	< hard > 519
158	00 : 44 : 04.0	+ 41 : 44 : 24	pn	pl	0.6 $^{+0.8}_{-0.3}$	2.4 $^{+1.6}_{-1.0}$	1.66 (0.85)	< hard > 521
159	00 : 44 : 04.9	+ 41 : 21 : 28	mos	br	7 $^{+8}_{-5}$	0.7 $^{+1.9}_{-0.7}$	58.3 (58.2)	< AGN > 524
160	00 : 44 : 06.5	+ 41 : 38 : 57	mos	pl	f	1.0 $^{+0.6}_{-0.7}$	1.41 (0.73)	< hard > 525
161	00 : 44 : 07.8	+ 41 : 56 : 07		faint			1.020	< hard > 528
162	00 : 44 : 10.1	+ 41 : 33 : 45	pn & mos	pl	f	3.7 $^{+1.0}_{-0.9}$	0.73 (0.51) / 0.56 (0.39)	< hard > 532
163	00 : 44 : 12.0	+ 41 : 31 : 50	pn & mos	pl	0.13 $^{+0.05}_{-0.07}$	2.0 $^{+0.2}_{-0.2}$	2.84 (0.52) / 2.78 (0.44)	< hard > 535
164	00 : 44 : 12.1	+ 41 : 45 : 13	pn & mos	pl	f	1.9 $^{+0.6}_{-0.6}$	1.50 (0.83) / 1.32 (0.65)	< hard > 536
165	00 : 44 : 13.2	+ 41 : 56 : 52		faint			1.528	< hard > 539
166	00 : 44 : 15.9	+ 41 : 30 : 59	pn & mos	pl	0.9 $^{+0.5}_{-0.3}$	1.3 $^{+0.3}_{-0.2}$	11.8 (1.7) / 11.7 (2.0)	XRB544
167	00 : 44 : 16.5	+ 41 : 26 : 29		faint			0.207	< fgstar > 545
168	00 : 44 : 17.9	+ 41 : 50 : 24		faint			0.575	< fgstar > 546
169	00 : 44 : 18.3	+ 41 : 51 : 33		faint			1.202	< hard > 547
170	00 : 44 : 18.9	+ 41 : 32 : 11	mos	pl	1.4 $^{+6.8}_{-1.3}$	2.8 $^{+4.4}_{-1.5}$	1.79 (1.34)	< hard > 548
171	00 : 44 : 20.0	+ 41 : 34 : 07	pn & mos	pl	f	2.2 $^{+0.4}_{-0.4}$	0.50 (0.23) / 0.44 (0.18)	< hard > 549
172	00 : 44 : 20.7	+ 41 : 35 : 43	pn & mos	pl	f	1.1 $^{+0.6}_{-0.6}$	1.26 (0.91) / 1.09 (0.73)	< hard > 550
173	00 : 44 : 22.9	+ 41 : 45 : 07	pn & mos	pl	f	1.93 $^{+0.13}_{-0.12}$	7.59 (1.20) / 13.9 (1.43)	< hard > 551
174	00 : 44 : 23.7	+ 42 : 00 : 08	pn	bb	f	0.16 $^{+0.04}_{-0.03}$	1.17 (0.82)	< fgstar > 553
175	00 : 44 : 24.7	+ 41 : 32 : 01	pn & mos	pl	0.20 $^{+0.04}_{-0.06}$	1.92 $^{+0.10}_{-0.15}$	5.92 (0.79) / 6.36 (0.65)	< hard > 555
176	00 : 44 : 25.5	+ 41 : 36 : 35	pn & mos	bb	0.24 $^{+0.11}_{-0.09}$	0.16 $^{+0.02}_{-0.02}$	4.84 (0.71) / 4.58 (0.79)	< fgstar > 556
177	00 : 44 : 25.8	+ 41 : 30 : 35	pn & mos	pl	0.24 $^{+0.20}_{-0.13}$	2.6 $^{+1.0}_{-0.4}$	1.95 (0.60) / 2.02 (0.62)	< hard > 558
178	00 : 44 : 28.0	+ 41 : 42 : 09	pn	br	f	0.4 $^{+0.5}_{-0.4}$	4.71 (1.03)	< hard > 561
179	00 : 44 : 29.5	+ 41 : 54 : 49		faint			-	< hard > ¹
180	00 : 44 : 30.4	+ 41 : 40 : 40		faint			0.399	< hard > 563
181	00 : 44 : 30.6	+ 41 : 23 : 06	mos	bb	f	0.7 $^{+0.3}_{-0.2}$	1.67 (1.06)	< hard > 564
182	00 : 44 : 32.2	+ 41 : 25 : 23	pn	pl	f	2.5 $^{+1.2}_{-1.0}$	1.18 (0.76)	fgStar565

Table A.1. continued.

Source	RA (J2000)	Dec (J2000)	Camera	Best Fit Model	n_{H} / 10^{22} cm^{-2}	Γ/kT keV	Luminosity / $10^{36} \text{ erg s}^{-1}$	Classification
183	00 : 44 : 33.5	+ 42 : 06 : 07		faint			1.240	< hard > 567
184	00 : 44 : 36.4	+ 41 : 25 : 31		faint			0.134	< hard > ¹
185	00 : 44 : 36.8	+ 42 : 04 : 36	pn	pl	0.3 $^{+1.1}_{-0.3}$	1.1 $^{+1.3}_{-0.8}$	4.91 (2.46)	< hard > 569
186	00 : 44 : 37.8	+ 41 : 45 : 15	pn & mos	pl	0.16 $^{+0.06}_{-0.07}$	2.2 $^{+0.3}_{-0.2}$	7.69 (1.21) / 9.02 (1.19)	< AGN > 570
187	00 : 44 : 37.9	+ 41 : 45 : 14	mos	pl	0.12 $^{+0.21}_{-0.12}$	2.2 $^{+0.7}_{-0.6}$	5.77 (1.73)	< AGN > 570
188	00 : 44 : 38.0	+ 41 : 40 : 09	pn & mos	pl	f	8 $^{+2}_{-8}$	44.3 (43.5) / 62.4 (61.5)	< hard > ¹
189	00 : 44 : 38.7	+ 41 : 31 : 47	pn & mos	pl	0.6 $^{+0.2}_{-0.3}$	2.2 $^{+2.9}_{-1.2}$	1.11 (0.76) / 1.55 (1.16)	< hard > 573
190	00 : 44 : 42.7	+ 41 : 53 : 41	pn & mos	pl	6 $^{+9}_{-4}$	0.4 $^{+1.4}_{-0.9}$	8.43 (5.94) / 14.8 (9.65)	< hard > 577
191	00 : 44 : 43.3	+ 41 : 26 : 28	pn	pl	f	3.7 $^{+1.6}_{-1.1}$	1.23 (0.93)	< hard > ¹
192	00 : 44 : 43.6	+ 41 : 46 : 47		faint			1.084	< AGN > ?
193	00 : 44 : 44.8	+ 41 : 51 : 55	pn & mos	pl	f	1.6 $^{+0.5}_{-0.4}$	3.12 (1.20) / 3.10 (1.16)	< hard > 581
194	00 : 44 : 45.1	+ 41 : 46 : 45		faint			0.156	< AGN > 580
195	00 : 44 : 46.0	+ 41 : 42 : 22	pn & mos	bb	f	1.4 $^{+1.4}_{-0.5}$	1.62 (1.47) / 2.93 (2.50)	< hard > 582
196	00 : 44 : 47.2	+ 41 : 29 : 21		faint			0.260	SNR583
197	00 : 44 : 47.3	+ 41 : 44 : 14	pn & mos	pl	f	1.0 $^{+0.8}_{-0.7}$	4.55 (3.98) / 2.88 (2.04)	< hard > 584
198	00 : 44 : 48.8	+ 41 : 58 : 13		faint			1.386	< hard > 586
199	00 : 44 : 49.3	+ 41 : 47 : 27		faint			1.465	< hard > 588
200	00 : 44 : 49.6	+ 41 : 47 : 28	pn	pl	f	2	1.47 (0.97)	< hard > 588
201	00 : 44 : 50.9	+ 41 : 29 : 06	pn & mos	pl	f	3.0 $^{+0.3}_{-0.3}$	2.15 (0.74) / 2.14 (0.59)	SNR589
202	00 : 44 : 51.3	+ 41 : 27 : 11	pn & mos	pl	f	1.9 $^{+0.2}_{-0.2}$	4.18 (1.20) / 8.82 (1.98)	< hard > ¹
203	00 : 44 : 51.5	+ 41 : 38 : 33	pn	pl	f	2.1 $^{+6.4}_{-1.9}$	2.76 (2.61)	< fgstar > 590
204	00 : 44 : 53.2	+ 42 : 02 : 15		faint			0.178	< fgstar > 593
205	00 : 44 : 55.3	+ 41 : 34 : 41	pn & mos	pl	0.5 $^{+0.2}_{-0.1}$	1.8 $^{+0.2}_{-0.2}$	10.3 (1.9) / 10.7 (1.6)	< AGN > 595
206	00 : 44 : 56.4	+ 41 : 59 : 37	pn & mos	br	0.17 $^{+0.12}_{-0.07}$	0.49 $^{+0.18}_{-0.16}$	4.02 (0.85) / 3.37 (0.95)	< fgstar > 598
207	00 : 44 : 58.4	+ 41 : 46 : 23	pn	pl	f	2.0 $^{+1.8}_{-1.2}$	2.77 (2.55)	< hard > 602
208	00 : 44 : 58.5	+ 41 : 46 : 21		faint			1.029	< hard > 602
209	00 : 44 : 59.2	+ 41 : 40 : 06	pn	bb	f	0.8 $^{+199}_{-0.8}$	0.66 (0.6)	< hard > 603

Table A.1. continued.

Source	RA (J2000)	Dec (J2000)	Camera	Best Fit Model	n_{H} / 10^{22} cm $^{-2}$	Γ/kT keV	Luminosity / 10^{36} erg s $^{-1}$	Classification
210	00 : 45 : 00.5	+ 41 : 27 : 04	pn	pl	$0.5^{+1.1}_{-0.4}$	$2.7^{+2.2}_{-0.7}$	2.82 (1.34)	< hard > 606
211	00 : 45 : 01.2	+ 41 : 56 : 09		faint			1.036	< AGN > 607
212	00 : 45 : 06.3	+ 42 : 06 : 19		faint			4.461	< hard > 612
213	00 : 45 : 06.9	+ 42 : 03 : 00	pn	pl	f	$0.6^{+0.6}_{-0.5}$	2.23 (1.67)	< AGN > 614
214	00 : 45 : 07.4	+ 41 : 53 : 56		faint			1.432	< fgstar > 615
215	00 : 45 : 09.8	+ 42 : 02 : 38	mos	br	f	$0.36^{+0.15}_{-0.13}$	2.86 (2.26)	< fgstar > 616
216	00 : 45 : 11.6	+ 41 : 45 : 59	pn & mos	pl	$0.15^{+0.28}_{-0.15}$	$1.6^{+0.5}_{-0.6}$	3.77 (1.14) / 2.38 (0.89)	< hard > 617
217	00 : 45 : 13.6	+ 41 : 35 : 30		faint			0.256	< hard > ¹
218	00 : 45 : 13.8	+ 41 : 36 : 17	pn & mos	br	$0.38^{+0.08}_{-0.14}$	$0.24^{+0.06}_{-0.04}$	39.6 (38.4) / 52.3 (51.3)	SNR621
219	00 : 45 : 15.1	+ 41 : 50 : 36	pn	bb	f	$0.22^{+0.09}_{-0.06}$	0.62 (0.44)	< hard > 622
220	00 : 45 : 18.5	+ 41 : 39 : 35	pn	pl	2^{+6}_{-2}	$1.5^{+3.6}_{-1.8}$	2.54 (2.35)	< hard > 626
221	00 : 45 : 19.7	+ 42 : 09 : 08		faint			0.471	< fgstar > 628
222	00 : 45 : 23.4	+ 41 : 51 : 58	pn	pl	f	$0.3^{+0.7}_{-0.8}$	2.47 (1.84)	< hard > 632
223	00 : 45 : 25.6	+ 41 : 53 : 29		faint			1.014	< hard > 633
224	00 : 45 : 26.1	+ 41 : 44 : 30		faint			0.769	< hard > 635
225	00 : 45 : 26.1	+ 41 : 43 : 12		faint			0.925	< hard > 634
226	00 : 45 : 26.7	+ 41 : 56 : 33	pn	pl	f	$0.9^{+0.9}_{-0.9}$	1.66 (1.32)	< hard > 636
227	00 : 45 : 27.1	+ 42 : 00 : 17	pn	pl	$0.4^{+1.7}_{-0.4}$	$2.0^{+5.6}_{-1.1}$	1.91 (1.15)	< hard > 637
228	00 : 45 : 28.3	+ 41 : 46 : 05		faint			1.081	< SNR > 642
229	00 : 45 : 31.2	+ 42 : 01 : 44	pn	bb	2^{+10}_{-2}	$0.6^{+0.6}_{-0.4}$	1.94 (1.93)	< hard > 645
230	00 : 45 : 31.3	+ 42 : 12 : 48		faint			0.578	< hard > 647
231	00 : 45 : 32.5	+ 41 : 55 : 07	mos	pl	1^{+14}_{-1}	$1.6^{+8.4}_{-1.8}$	1.65 (1.40)	< hard > 648
232	00 : 45 : 33.0	+ 42 : 10 : 58	pn & mos	pl	$0.6^{+1.2}_{-0.4}$	4^{+6}_{-2}	10.9 (8.3) / 8.40 (6.81)	< fgstar > 649
233	00 : 45 : 33.5	+ 42 : 08 : 07		faint			0.422	< hard > 650
234	00 : 45 : 34.7	+ 42 : 17 : 49	mos	pl	f	$0.9^{+0.7}_{-0.6}$	3.56 (2.45)	< hard > 652
235	00 : 45 : 35.5	+ 42 : 20 : 32	pn & mos	pl	$0.17^{+0.57}_{-0.17}$	$1.7^{+1.7}_{-0.9}$	1.72 (1.02) / 2.45 (1.38)	< hard > 654
236	00 : 45 : 38.0	+ 42 : 12 : 33	mos	pl	f	$0.9^{+0.6}_{-0.5}$	2.97 (1.95)	< hard > 661

Table A.1. continued.

Source	RA (J2000)	Dec (J2000)	Camera	Best Fit Model	n_{H} / 10^{22} cm $^{-2}$	Γ/kT keV	Luminosity / 10^{36} erg s $^{-1}$	Classification
237	00 : 45 : 38.8	+ 41 : 56 : 16		faint		$^+_{-}$	1.235	< fgstar > 662
238	00 : 45 : 40.3	+ 42 : 08 : 05	pn & mos	diskbb	0.13 $^{+0.07}_{-0.07}$	0.25 $^{+0.05}_{-0.05}$	37.1 (11.71) / 38.8 (14.7)	< fgstar > 663
239	00 : 45 : 40.5	+ 42 : 08 : 07	pn & mos	bb	f	0.17 $^{+0.01}_{-0.01}$	11.6 (2.1) / 11.4 (1.9)	< fgstar > 663
240	00 : 45 : 41.7	+ 42 : 23 : 24	pn & mos	pl	0.12 $^{+0.57}_{-0.12}$	2.6 $^{+3.7}_{-1.2}$	1.29 (0.71) / 1.09 (0.71)	< hard > 666
241	00 : 45 : 42.8	+ 42 : 14 : 20	pn	pl	0.8 $^{+1.7}_{-0.6}$	3.7 $^{+6.1}_{-1.7}$	8.17 (7.41)	< hard > 670
242	00 : 45 : 43.8	+ 42 : 08 : 42		faint			0.771	< hard > 1
243	00 : 45 : 44.1	+ 42 : 08 : 44		faint			0.496	< hard > 1
244	00 : 45 : 44.8	+ 41 : 58 : 58	pn	pl	0.33 $^{+0.19}_{-0.17}$	2.0 $^{+0.6}_{-0.4}$	5.48 (1.22)	< hard > 673
245	00 : 45 : 45.5	+ 41 : 49 : 33		faint			0.870	< hard > 674
246	00 : 45 : 45.8	+ 41 : 50 : 30		faint			1.236	< fgstar > 675
247	00 : 45 : 50.9	+ 41 : 58 : 34		faint			1.046	< hard > 1
248	00 : 45 : 51.5	+ 42 : 04 : 20		faint			1.020	< hard > 682
249	00 : 45 : 53.4	+ 42 : 16 : 10	pn	br	f	0.5 $^{+0.9}_{-0.2}$	0.63 (0.53)	< hard > 1
250	00 : 45 : 54.7	+ 42 : 13 : 11		faint			0.109	< hard > 1
251	00 : 45 : 55.2	+ 41 : 52 : 11		faint			1.238	< hard > 687
252	00 : 45 : 56.0	+ 42 : 12 : 33	pn & mos	pl	0.3 $^{+1.3}_{-0.3}$	2.6 $^{+0.7}_{-1.4}$	1.58 (0.79) / 1.52 (0.85)	< hard > 690
253	00 : 45 : 56.9	+ 41 : 48 : 32		faint			0.793	< hard > 1
254	00 : 45 : 57.9	+ 42 : 26 : 47	pn & mos	pl	f	2.3 $^{+0.4}_{-0.3}$	5.31 (1.54) / 5.43 (1.11)	< hard > 694
255	00 : 45 : 58.2	+ 42 : 02 : 59	pn	pl	f	2.0 $^{+0.7}_{-0.6}$	3.25 (1.63)	< fgstar > 693
256	00 : 45 : 58.8	+ 42 : 04 : 25	pn & mos	pl	0.3 $^{+0.4}_{-0.2}$	1.2 $^{+0.4}_{-0.5}$	4.68 (1.64) / 6.04 (2.10)	< hard > 696
257	00 : 45 : 59.0	+ 42 : 04 : 21		faint			0.602	< hard > 696
258	00 : 46 : 00.2	+ 42 : 10 : 31	pn & mos	pl	f	0.03 $^{+0.7}_{-0.8}$	4.22 (3.18) / 3.64 (2.63)	< hard > 698
259	00 : 46 : 02.9	+ 42 : 24 : 31	pn & mos	pl	0.3 $^{+0.3}_{-0.1}$	3.8 $^{+1.5}_{-0.9}$	3.20 (1.82) / 4.21 (2.18)	< fgstar > 701
260	00 : 46 : 03.6	+ 42 : 13 : 22		faint			0.284	< hard > 1
261	00 : 46 : 04.6	+ 41 : 49 : 47		faint			0.982	< SNR > 704
262	00 : 46 : 05.1	+ 41 : 51 : 44		faint			1.186	< hard > 705
263	00 : 46 : 05.1	+ 42 : 25 : 52	mos	pl	5 $^{+12}_{-5}$	0.3 $^{+2.4}_{-1.5}$	6.69 (6.08)	< hard > 706

Table A.1. continued.

Source	RA (J2000)	Dec (J2000)	Camera	Best Fit Model	n_{H} / 10^{22} cm $^{-2}$	Γ/kT keV	Luminosity / 10^{36} erg s $^{-1}$	Classification
264	00 : 46 : 05.5	+ 42 : 20 : 29	pn & mos	pl	0.7 $^{+1.8}_{-0.6}$	2.0 $^{+3.2}_{-1.0}$	1.38 (0.92) / 1.82 (1.23)	< AGN > 707
265	00 : 46 : 08.2	+ 42 : 10 : 53	mos	bb	0.3 $^{+1.5}_{-0.3}$	1.0 $^{+0.5}_{-0.3}$	1.50 (1.23)	< hard > 715
266	00 : 46 : 08.9	+ 42 : 29 : 39		faint			0.472	< hard > 716
267	00 : 46 : 09.5	+ 42 : 15 : 45		faint			0.221	< hard > 717
268	00 : 46 : 11.4	+ 41 : 59 : 03	pn	pl	0.3 $^{+0.6}_{-0.3}$	2.3 $^{+3.2}_{-1.3}$	2.58 (1.33)	< hard > 720
269	00 : 46 : 11.7	+ 42 : 08 : 25	pn & mos	pl	0.3 $^{+0.1}_{-0.1}$	1.7 $^{+0.1}_{-0.2}$	9.54 (2.04) / 11.1 (1.58)	< hard > 721
270	00 : 46 : 12.1	+ 42 : 08 : 27	pn	pl	f	1.4 $^{+0.5}_{-0.5}$	6.86 (2.77)	< hard > 721
271	00 : 46 : 12.5	+ 42 : 21 : 51	pn & mos	pl	0.2 $^{+0.2}_{-0.1}$	1.3 $^{+0.3}_{-0.3}$	2.52 (0.89) / 3.81 (0.88)	< hard > 723
272	00 : 46 : 12.6	+ 42 : 10 : 26		faint			0.558	< hard > 722
273	00 : 46 : 13.6	+ 41 : 50 : 41	pn	pl	f	1.8 $^{+1.0}_{-0.7}$	3.38 (1.89)	< hard > 724
274	00 : 46 : 13.6	+ 42 : 12 : 13		faint			0.261	< hard > 1
275	00 : 46 : 16.4	+ 42 : 21 : 28	pn & mos	pl	f	1.6 $^{+0.4}_{-0.3}$	1.24 (0.58) / 1.67 (0.65)	< hard > 728
276	00 : 46 : 18.3	+ 42 : 25 : 36	pn & mos	pl	0.18 $^{+0.11}_{-0.12}$	2.1 $^{+0.7}_{-0.4}$	2.57 (0.76) / 2.82 (0.72)	< hard > 731
277	00 : 46 : 18.9	+ 42 : 15 : 54	pn & mos	bb	f	11 $^{+10}_{-8}$	4.29 (3.94) / 4.22 (3.93)	< AGN > 732
278	00 : 46 : 19.9	+ 42 : 14 : 41	pn & mos	pl	0.14 $^{+0.07}_{-0.08}$	1.6 $^{+0.2}_{-0.2}$	5.95 (1.96) / 6.20 (1.14)	< hard > 735
279	00 : 46 : 21.9	+ 42 : 01 : 46		faint			0.812	< hard > 1
280	00 : 46 : 24.9	+ 42 : 04 : 22	pn & mos	pl	0.33 $^{+0.03}_{-0.03}$	1.98 $^{+0.09}_{-0.08}$	89 (6) / 109 (5)	< hard > 1
281	00 : 46 : 25.3	+ 42 : 24 : 41	pn & mos	pl	0.7 $^{+0.7}_{-0.4}$	3.9 $^{+2.5}_{-0.9}$	6.05 (4.51) / 6.56 (4.80)	< hard > 750
282	00 : 46 : 25.5	+ 42 : 04 : 22	pn	pl	0.22 $^{+0.08}_{-0.05}$	1.74 $^{+0.22}_{-0.14}$	65.4 (6.7)	< hard > 1
283	00 : 46 : 26.9	+ 42 : 01 : 50	pn	pl	0.12 $^{+0.03}_{-0.02}$	1.41 $^{+0.08}_{-0.08}$	147 (9)	GIC752
284	00 : 46 : 27.0	+ 42 : 01 : 51	pn & mos	pl	0.12 $^{+0.02}_{-0.02}$	1.50 $^{+0.07}_{-0.07}$	146 (10) / 168 (8)	GIC752
285	00 : 46 : 30.8	+ 42 : 00 : 38		faint			1.441	< hard > 1
286	00 : 46 : 32.0	+ 41 : 51 : 25		faint			1.500	< hard > 1
287	00 : 46 : 32.4	+ 42 : 13 : 50	mos	pl	1.5 $^{+4.6}_{-1.4}$	2 $^{+8}_{-2}$	1.49 (1.34)	< hard > 757
288	00 : 46 : 34.7	+ 42 : 17 : 55	pn & mos	pl	0.9 $^{+1.0}_{-0.4}$	2.3 $^{+1.3}_{-0.5}$	1.64 (0.86) / 1.88 (0.89)	< hard > 758
289	00 : 46 : 37.4	+ 42 : 16 : 20	pn & mos	br	f	0.5 $^{+0.3}_{-0.2}$	0.43 (0.35) / 0.41 (0.35)	< fgstar > 764
290	00 : 46 : 40.2	+ 42 : 25 : 20	pn & mos	pl	0.25 $^{+0.11}_{-0.12}$	3.6 $^{+0.7}_{-1.2}$	4.81 (2.81) / 4.95 (2.35)	< fgstar > 770

Table A.1. continued.

Source	RA (J2000)	Dec (J2000)	Camera	Best Fit Model	n_{H} / 10^{22} cm^{-2}	Γ/kT keV	Luminosity / $10^{36} \text{ erg s}^{-1}$	Classification
291	00 : 46 : 40.7	+ 41 : 54 : 23	pn	br	3^{+6}_{-2}	$0.6^{+7.2}_{-0.6}$	18.5 (18.5)	< AGN > 771
292	00 : 46 : 42.5	+ 42 : 20 : 51		faint			0.493	< hard > 775
293	00 : 46 : 43.1	+ 42 : 13 : 37	pn	pl	2^{+46}_{-2}	$1.2^{+5.5}_{-2.0}$	1.37 (1.29)	< hard > 776
294	00 : 46 : 43.4	+ 42 : 09 : 48	pn & mos	pl	f	$1.1^{+0.4}_{-0.3}$	1.89 (1.02) / 1.40 (0.65)	< hard > 777
295	00 : 46 : 45.1	+ 42 : 27 : 18	pn & mos	pl	f	$1.1^{+0.7}_{-0.5}$	2.50 (1.61) / 1.18 (0.90)	< hard > ¹
296	00 : 46 : 48.0	+ 42 : 08 : 52	pn & mos	pl	$0.4^{+0.1}_{-0.1}$	$2.0^{+0.2}_{-0.2}$	8.03 (1.41) / 9.77 (1.30)	< AGN > 784
297	00 : 46 : 49.2	+ 42 : 09 : 30	mos	pl	f	$4.3^{+2.4}_{-1.6}$	2.40 (1.81)	< fgstar > 787
298	00 : 46 : 49.4	+ 42 : 25 : 25		faint			0.238	< hard > 788
299	00 : 46 : 51.7	+ 42 : 19 : 49	pn & mos	pl	$0.2^{+0.1}_{-0.1}$	$1.8^{+0.4}_{-0.3}$	2.32 (0.57) / 2.50 (0.51)	< hard > 789
300	00 : 46 : 51.8	+ 42 : 15 : 5	pn & mos	pl	f	$1.8^{+0.4}_{-0.3}$	1.54 (0.71) / 1.99 (0.70)	< hard > 790
301	00 : 46 : 52.1	+ 42 : 17 : 10	pn & mos	pl	$0.3^{+0.4}_{-0.2}$	$2.2^{+0.7}_{-0.8}$	2.4 (1.1) / 1.6 (0.8)	< hard > 792
302	00 : 46 : 53.4	+ 42 : 19 : 13	pn	pl	f	$0.9^{+0.6}_{-0.6}$	1.06 (0.74)	< hard > 794
303	00 : 46 : 54.4	+ 42 : 10 : 18	pn & mos	pl	$1.4^{+0.9}_{-0.6}$	$2.2^{+0.9}_{-0.5}$	4.33 (1.52) / 4.80 (1.91)	< hard > 795
304	00 : 46 : 55.2	+ 42 : 20 : 48	pn & mos	pl	$0.15^{+0.01}_{-0.01}$	$2.25^{+0.07}_{-0.06}$	43 (2) / 53 (2)	< hard > 796
305	00 : 46 : 58.4	+ 42 : 24 : 13	pn	pl	f	$1.1^{+0.8}_{-0.7}$	2.03 (1.40)	< fgstar > 800
306	00 : 46 : 59.6	+ 42 : 18 : 06		faint			0.282	< hard > ¹
307	00 : 47 : 00.4	+ 42 : 21 : 55	pn	bb	f	$0.15^{+0.03}_{-0.02}$	0.86 (0.53)	< fgstar > 802
308	00 : 47 : 01.9	+ 42 : 22 : 46	pn & mos	pl	f	$1.7^{+0.5}_{-0.4}$	1.09 (0.58) / 0.86 (0.39)	< hard > 804
309	00 : 47 : 02.6	+ 42 : 18 : 35	pn & mos	pl	$0.2^{+0.2}_{-0.2}$	$2.5^{+0.6}_{-1.0}$	1.26 (0.38) / 1.28 (0.39)	< hard > 805
310	00 : 47 : 03.6	+ 42 : 04 : 48	pn & mos	pl	$0.2^{+0.2}_{-0.1}$	$1.6^{+0.4}_{-0.3}$	7.90 (2.04) / 6.91 (1.45)	< hard > 808
311	00 : 47 : 04.3	+ 42 : 16 : 47		faint			0.533	< hard > 812
312	00 : 47 : 06.3	+ 42 : 22 : 09	pn & mos	pl	$0.41^{+0.19}_{-0.12}$	$1.8^{+0.3}_{-0.2}$	5.02 (1.03) / 6.27 (0.95)	< hard > 817
313	00 : 47 : 07.6	+ 42 : 18 : 10	pn & mos	pl	$0.6^{+0.5}_{-0.2}$	$1.9^{+0.6}_{-0.3}$	2.65 (0.81) / 2.77 (0.78)	< hard > 820
314	00 : 47 : 08.6	+ 42 : 24 : 04	pn & mos	pl	$0.39^{+0.28}_{-0.15}$	$2.0^{+0.2}_{-0.4}$	4.21 (1.21) / 3.03 (0.88)	< hard > 821
315	00 : 47 : 09.0	+ 42 : 10 : 09	mos	bb	f	2^{+198}_{-1}	11.2 (10.2)	< hard > 822
316	00 : 47 : 10.5	+ 42 : 18 : 45	mos	pl	f	$1.7^{+0.8}_{-0.6}$	1.10 (0.64)	< hard > 824
317	00 : 47 : 10.8	+ 42 : 16 : 13	pn	pl	f	$2.3^{+1.9}_{-1.4}$	1.09 (0.98)	< hard > 825

Table A.1. continued.

Source	RA (J2000)	Dec (J2000)	Camera	Best Fit Model	n_{H} / 10^{22} cm^{-2}	Γ/kT keV	Luminosity / $10^{36} \text{ erg s}^{-1}$	Classification
318	00 : 47 : 11.3	+ 42 : 22 : 22	pn & mos	pl	$3.4^{+2.6}_{-1.5}$	$3.0^{+1.4}_{-0.7}$	5.85 (4.03) / 8.87 (6.45)	< hard > 826
319	00 : 47 : 13.2	+ 42 : 20 : 44	pn & mos	pl	$0.14^{+0.06}_{-0.06}$	$2.1^{+0.2}_{-0.2}$	6.97 (1.10) / 8.27 (0.89)	< hard > 827
320	00 : 47 : 21.0	+ 42 : 05 : 47	pn & mos	br	$0.48^{+0.17}_{-0.42}$	$0.18^{+0.25}_{-0.09}$	9.07 (9.07) / 5.65 (5.65)	< fgstar > 835
321	00 : 47 : 24.0	+ 42 : 08 : 43		faint			0.402	< hard > 837
322	00 : 47 : 25.2	+ 42 : 21 : 16	pn & mos	pl	$0.19^{+0.07}_{-0.09}$	$2.2^{+0.2}_{-0.3}$	3.15 (0.74) / 3.95 (0.77)	< hard > 839
323	00 : 47 : 26.0	+ 42 : 21 : 57	pn & mos	br	$0.96^{+0.05}_{-0.05}$	$0.12^{+0.03}_{-0.02}$	538 (524) / 605 (593)	< fgstar > 840
324	00 : 47 : 27.4	+ 42 : 13 : 46	pn & mos	br	$2.7^{+3.3}_{-1.5}$	$1.4^{+2.6}_{-1.4}$	2.18 (2.18) / 2.57 (2.57)	< hard > 842
325	00 : 47 : 30.5	+ 42 : 12 : 01		faint			0.611	< hard > ¹
326	00 : 47 : 35.9	+ 42 : 08 : 34	pn & mos	pl	$0.12^{+0.31}_{-0.12}$	$1.3^{+0.9}_{-0.6}$	3.30 (1.72) / 3.40 (1.43)	< hard > 845
327	00 : 47 : 38.4	+ 42 : 20 : 21	mos	pl	$0.11^{+0.25}_{-0.11}$	$1.4^{+0.7}_{-0.5}$	4.78 (1.42)	< AGN > 846
328	00 : 47 : 42.5	+ 42 : 22 : 27	mos	pl	f	$1.9^{+0.5}_{-0.4}$	3.92 (1.43)	< hard > 848
329	00 : 47 : 42.6	+ 42 : 11 : 38	pn & mos	pl	$0.2^{+0.3}_{-0.2}$	$1.8^{+0.6}_{-0.6}$	1.93 (0.95) / 2.09 (0.72)	< hard > 849
330	00 : 47 : 42.7	+ 42 : 10 : 15		faint			0.618	< hard > 850
331	00 : 47 : 43.7	+ 42 : 12 : 19		faint			0.747	< hard > 851
332	00 : 47 : 44.4	+ 42 : 10 : 58	pn & mos	pl	$0.23^{+0.22}_{-0.16}$	$2.0^{+0.4}_{-0.5}$	2.52 (0.98) / 3.93 (1.14)	< hard > 852
333	00 : 47 : 46.5	+ 42 : 18 : 49		faint			0.821	< hard > ¹
334	00 : 47 : 46.9	+ 42 : 14 : 22	mos	pl	$0.7^{+1.1}_{-0.5}$	$2.7^{+1.9}_{-1.6}$	3.72 (2.71)	< hard > 853
335	00 : 47 : 48.1	+ 42 : 19 : 33	mos	pl	$0.21^{+0.09}_{-0.08}$	$1.6^{+0.2}_{-0.2}$	60.8 (5.30)	< AGN > 855